Fermilab FERMILAB-PUB-05-016-CD FEBRUARY 2005

The SDSS View of the Palomar-Green Bright Quasar Survey

Sebastian Jester,[1] Donald P. Schneider,[2] Gordon T. Richards,[3] Richard F. Green,[4] Maarten Schmidt,[5] Patrick B. Hall,[6] Michael A. Strauss,[3] Daniel E. Vanden Berk,[3] Chris Stoughton,[1] James E. Gunn,[3] Jon Brinkmann,[7] Stephen M. Kent,[1,8] J. Allyn Smith,[9,10] Douglas L. Tucker,[1] and Brian Yanny[1]

ABSTRACT

We investigate the extent to which the Palomar-Green (PG) Bright Quasar Survey (BQS) is complete and representative of the general quasar population by comparing with imaging and spectroscopy from the Sloan Digital Sky Survey. A comparison of SDSS and PG photometry of both stars and quasars reveals the need to apply a color and magnitude recalibration to the PG data. Using the SDSS photometric catalog, we define the PG's parent sample of objects that are not main-sequence stars and simulate the selection of objects from this parent sample using the PG photometric criteria and errors. This simulation shows that the effective $U-B$ cut in the PG survey is $U-B < -0.71$, implying a color-related incompleteness. As the color distribution of bright quasars peaks near $U-B = -0.7$ and the 2-σ error in $U-B$ is comparable to the full width

[1]Fermi National Accelerator Laboratory, P.O. Box 500, Batavia, IL 60510.

[2]Department of Astronomy and Astrophysics, The Pennsylvania State University, 525 Davey Laboratory, University Park, PA 16802.

[3]Princeton University Observatory, Peyton Hall, Princeton, NJ 08544.

[4]Kitt Peak National Observatory, National Optical Astronomy Observatories, P.O. Box 26732, 950 North Cherry Avenue, Tucson, AZ 85726

[5]Department of Astronomy, MC 105-24, California Institute of Technology, 1200 East California Boulevard, Pasadena, CA 91125.

[6]Department of Physics and Astronomy, York University, 4700 Keele St., Toronto, Ontario M3J 1P3, Canada

[7]Apache Point Observatory, P.O. Box 59, Sunspot, NM 88349.

[8]Department of Astronomy and Astrophysics, The University of Chicago, 5640 South Ellis Avenue, Chicago, IL 60637.

[9]Department of Physics and Astronomy, University of Wyoming, P.O. Box 3905, Laramie, WY 82071.

[10]Los Alamos National Laboratory, P.O. Box 1663, Los Alamos, NM 87545.

of the color distribution of quasars, the color incompleteness of the BQS is approximately 50% and essentially random with respect to $U-B$ color for $z < 0.5$. There is, however, a bias against bright quasars at $0.5 < z < 1$, which is induced by the color-redshift relation of quasars (although quasars at $z > 0.5$ are inherently rare in bright surveys in any case). We find no evidence for any other systematic incompleteness when comparing the distributions in color, redshift, and FIRST radio properties of the BQS and a BQS-like subsample of the SDSS quasar sample. However, the application of a bright magnitude limit biases the BQS toward the inclusion of blue objects, in particular compared to the full range of colors found among the SDSS quasars. Furthermore, the i-band limited SDSS sample includes much redder objects than the BQS, even at i-band magnitudes comparable to those of the BQS objects.

Subject headings: Surveys — Catalogs — Quasars: general — Quasars: emission lines — Galaxies: active

1. Introduction

1.1. The Palomar-Green Bright Quasar Survey

The Bright Quasar Survey (BQS; Schmidt & Green 1983, hereafter referred to as SG83) is the set of quasars detected in the Palomar-Green (PG) survey of ultraviolet excess objects (Green et al. 1986, hereafter referred to as GSL86). The PG survey selects UV excess objects with $U-B < -0.46$ (corresponding to $U-B < -0.44$ for quasars with the mean color difference between stars and quasars assumed by SG83) brighter than an effective limiting magnitude of $B_{\rm lim} = 16.16$. The BQS was the first large-area homogeneous quasar survey, and it remains the largest-area survey for bright quasars at $B < 16$. Because of the UV excess criterion, it is primarily sensitive to quasars at redshifts up to $z = 2.2$, where the Lyman-α line enters the B-band and gives quasars very red $U-B$ colors ($U-B > 0$).

SG83 inferred strong luminosity evolution of quasars from a combination of the BQS and fainter small-area quasar surveys. However, a number of authors find a substantially larger number of bright UV excess quasars, implying that the BQS is substantially incomplete. For example, Goldschmidt et al. (1992) reported that the bright quasar surface density from the Edinburgh Quasar Survey is three times that found by the BQS, leading to very different volume densities of low-redshift high-luminosity quasars and hence different results on the evolution of the quasar luminosity function (Goldschmidt & Miller 1998). By contrast, Wisotzki et al. (2000) find that the BQS has a completeness of 68% compared to

the Hamburg-ESO quasar survey (HEQS). Next to the BQS, the HEQS is the largest-area survey reaching similarly bright magnitudes as the BQS, but only overlaps part of the PG survey area as it surveyed the Southern hemisphere.

Some authors have raised concerns that the BQS incompleteness may be systematic with respect to optical color or radio properties. For example, Wampler & Ponz (1985) have suggested that the paucity of BQS quasars in the redshift interval $0.5 < z < 1.0$ may be caused by a BQS bias against redder quasars (or "quasars with yellow $U-B$ colors", as designated by Wampler & Ponz 1985) — in this redshift interval, the passage of the MgII line through the B filter results in a $U-B$ color that is 0.2 mag redder than at lower and higher redshifts. However, Laor et al. (1997) have argued that a cut of $U-B < -0.44$ is red enough to avoid this bias. Based on independent photometry of the luminous ($M_B < -24$) BQS objects, Wampler & Ponz (1985) also suggested that some of the PG limiting magnitudes (which varied from plate to plate) might have been "much fainter than stated".

There are also concerns about a systematic incompleteness with respect to radio properties. Miller et al. (1993) found that 50% of $z < 0.5$ BQS quasars are steep-spectrum radio-loud objects; they cautioned that this number might be spuriously high if the BQS selection favored the inclusion of radio-luminous objects. This cautionary note was interpreted by Goldschmidt et al. (1999) and others as *suggesting* a radio-dependent incompleteness, casting doubts on the results obtained from statistical analyses of the radio properties of BQS objects.

In fact, PG quasars are often considered to be the archetype optically selected quasar sample, in particular when studying the properties of optically selected quasars at other wavelengths. Many other optically selected quasar surveys are now available which reach much fainter magnitudes and higher redshifts, use more general selection criteria, and generally have a much larger sample size (e.g., the Palomar Transit Grism Survey by Schneider et al. 1994 with 90 objects at $2.75 < z < 4.75$ over an area of $61.5\,\mathrm{deg}^2$; the Large Bright Quasar Survey by Hewett et al. 1995, 1055 objects with $16 < B_J < 18.9$ at $0.2 < z < 3.4$ over $454\,\mathrm{deg}^2$; COMBO-17 by Wolf et al. 2003, 192 objects with $17 < R < 24$ at $1.2 < z < 4.8$ over $0.78\,\mathrm{deg}^2$; the 2dF QSO redshift survey by Croom et al. 2004, 23 338 objects with $16 < b_\mathrm{J} < 20.85$ at $z < 3$ over $674\,\mathrm{deg}^2$); in particular, the SDSS quasar survey (Richards et al. 2002) has cataloged nearly 50,000 quasars so far, including of order 500 at $z > 4$ (Schneider et al. 2003; Schneider et al. 2005) and, in a separate search, 16 at $z > 5.7$ (Fan et al. 2004). Each of these surveys will be more or less biased towards or against objects with a particular class of SEDs.

Because of the historical importance of the BQS in general, and its key role in anchoring the bright end of the local quasar luminosity function in particular, we investigate here

whether the BQS suffers from any systematic incompleteness. By "incompleteness", we refer both to lack of objects that in fact pass the survey's magnitude and color limits, but also to the extent to which the survey is representative of quasars satisfying the broadest definition of the term (objects showing non-stellar continua and broad emission lines). We do so by comparing PG and Sloan Digital Sky Survey (SDSS; York et al. 2000) photometry of PG sources (§2), by considering the completeness of the PG UV excess sample relative to UV excess sources from SDSS (§3), and by comparing properties of BQS objects to those of "BQS-like" quasars from the SDSS (§4), with special attention to radio properties in §4.2.2. We also consider which part of the quasar population found by the SDSS are selected by the BQS criteria. In our discussion section, we compare our findings to previous investigations of the BQS incompleteness (§5.1) and consider the biases induced by the selection criteria of the BQS and other quasar surveys. §5.2 considers the more general question of how selection criteria bias our view of the general quasar population. We summarize our findings in §6.

1.2. Selection of objects in the BQS

For reference, we briefly review the construction of the BQS sample from SG83 and GSL86. The PG survey selects UV excess objects on double exposures of baked IIa-O photographic plates through filters U (using Schott UG-2) and B (GG-13) obtained using the Palomar 18 inch (46 cm) Schmidt telescope. The exposure times were adjusted to obtain equal image densities for objects with $U-B=-0.46$ (with the mean color difference between the spectral energy distribution [SED] of stars and quasars assumed by SG83, this translates to $U-B=-0.44$ for quasars). The magnitudes were calibrated using photoelectric calibration exposures of local standards. The calibration was stabilized by fitting a model of star counts as function of galactic coordinates. The limiting B magnitude varied from plate to plate; Figure 1 shows the distribution of limiting magnitudes. SG83 give an effective limiting magnitude of $B<16.16$ and photometric errors of $\sigma_B=0.27$ and $\sigma_{U-B}=0.24$. These were later revised by GSL86 to $\sigma_B=0.34$ and $\sigma_{U-B}=0.39$. The area covered by the complete PG survey was 10,668 deg^2.

UV excess candidates passing the photometric selection criteria were observed spectroscopically to determine quasar redshifts and to remove main-sequence objects that had been scattered into the sample. Conversely, some objects that had been confirmed spectroscopically as objects that are not main-sequence stars (hereafter called "off-main sequence objects") were retained in the PG sample even if the final photometric calibration formally caused them to fail the photometric selection criteria.

The BQS consists of 114 PG objects, which were required to have "dominant starlike

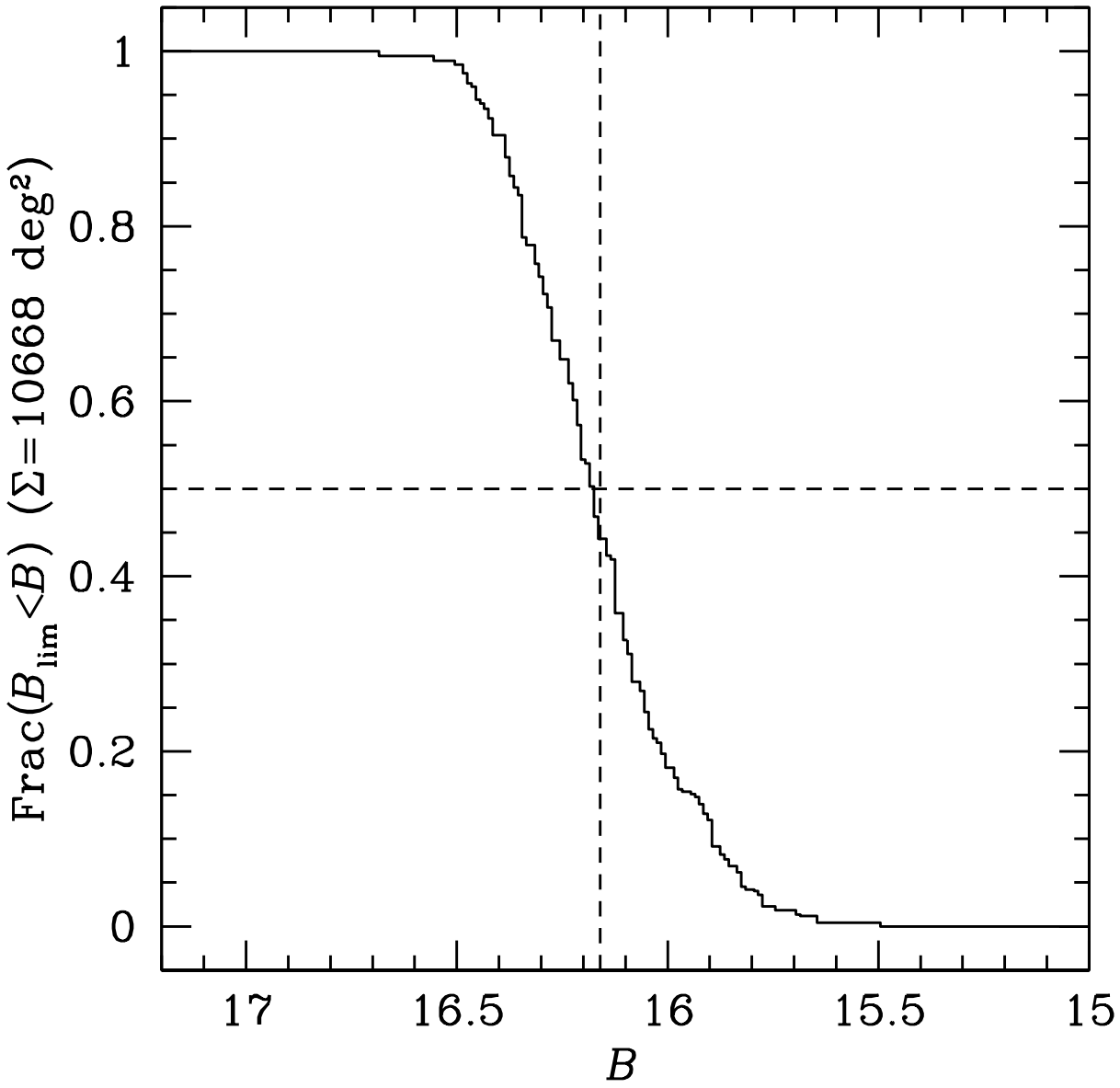

Fig. 1.— Area-weighted cumulative histogram of limiting magnitudes in the complete PG sample (using the areas and limiting magnitudes of PG survey plates from GSL86, Table 1). The effective limiting magnitude $B_{\rm eff} = 16.16$ given by SG83 and GSL86 is very close to the area-weighted median limiting magnitude as indicated by the dashed lines.

appearance on blue prints of the 48 inch (1.2 m) Schmidt Sky Atlas" (the Palomar Sky Survey) and "broad emission lines with substantial redshift" (SG83). Like all bright quasar surveys, the redshift distribution of BQS objects peaks at low redshift, with a median z of 0.176, and 88 out of 114 objects (77%) at $z < 0.5$.

1.3. The SDSS

The Sloan Digital Sky Survey (York et al. 2000; Stoughton et al. 2002) is a photometric and spectroscopic survey of the extragalactic sky at high galactic latitude visible from the northern hemisphere. In this paper, we use the data set published as Data Release 3 (DR3; Abazajian et al. 2004b)[1]. The DR3 photometric catalog covers $5282\,\mathrm{deg}^2$, while the DR3 spectroscopic catalog covers $4188\,\mathrm{deg}^2$. The SDSS uses a wide-field camera (Gunn et al. 1998) to obtain *ugriz* photometry (Fukugita et al. 1996; Lupton et al. 1999; Hogg et al. 2001; Lupton et al. 2001; Smith et al. 2002; Ivezić et al. 2004) with a photometric accuracy of 2–3%, a comparable precision of placing the photometry on the AB magnitude scale (Oke & Gunn 1983; Abazajian et al. 2004a), and with an astrometric accuracy of better than $0\farcs1$ (Pier et al. 2003). The SDSS is also a spectroscopic survey of complete samples of galaxies (Eisenstein et al. 2001; Strauss et al. 2002) and quasars. Quasar candidates are selected from SDSS photometry using an algorithm (Richards et al. 2002) targeting objects with non-stellar colors or that are point-source optical counterparts of FIRST (Becker et al. 1995) radio sources. A tiling algorithm ensures uniformity and efficiency of the allocation of fibers to quasar candidates and other spectroscopic targets (Blanton et al. 2003). A manually vetted quasar catalog based on DR3 data akin to that based on DR1 (Schneider et al. 2003) is given by Schneider et al. (2005) and contains over 46,000 quasars.

In this paper, we use $\Omega_\mathrm{m} = 0.3, \Omega_\Lambda = 0.7$, and $H_0 = 70\,\mathrm{km/s/Mpc}$.

2. The photometric properties of PG sources in the SDSS

To evaluate the photometric completeness of the BQS, we perform separate comparisons of the PG and SDSS photometry for stars and quasars[2]. The stellar photometry will be used to assess the photometric accuracy and precision of the PG survey using SDSS observations

[1]Available on-line at http://www.sdss.org/dr3/

[2]We use the term "quasar" here, but it should be understood as being synonymous with "QSO" without any implication about luminosity or presence of radio emission

of PG objects. The quasar photometry transformations will be used to define a sample of SDSS quasars satisfying the BQS color selection criteria.

The SDSS photometric system is based on a set of standard stars which includes stars as blue as PG objects (Smith et al. 2002). The PG survey reports photometry transformed to the Johnson U and B system. Since a subset of the SDSS standard stars is taken from the Landolt standard fields with Johnson-Kron-Cousins $UBVR_{\rm C}I_{\rm C}$ photometry (Landolt 1973, 1983, 1992), it is straightforward to establish color and magnitude transformations between the SDSS and the Landolt system. However, these transformations are not appropriate for quasars because of their different spectral shapes. Therefore, we determine separate color and magnitude transformations for quasars by performing synthetic photometry of composite quasar spectra in the SDSS and Landolt systems. We describe each process in turn.

2.1. Photometric transformation for stars

Fukugita et al. (1996) and Smith et al. (2002) give color and magnitude transformations (synthetic and observed) between the Landolt system and the system of the United States Naval Observatory (USNO) 1.0 m telescope (designated $u'g'r'i'z'$). We transform the USNO magnitudes of the SDSS standard stars to the system of the SDSS 2.5 m telescope (i.e., the SDSS *ugriz* system) using the equations given by Gunn (2003). We use only those standard stars with $U - B < 0$ and perform linear least squares fits to determine the transformations from the SDSS system to U and B. The resulting coefficients are given in Table 1. For reference in work with objects redder than $U - B = 0$, we also give the coefficients obtained using all SDSS standard stars with $R-I < 1.15$ (stars with $R-I < 1.15$ have different color transformations than those with $R-I \geq 1.15$, but there is no Landolt photometry of a sufficient number of SDSS standards with $R-I \geq 1.15$ for us to derive reliable transformations), as well as coefficients for transformations between other filters.

Table 1. Transformations between $ugriz$ and $UBVR_{\rm C}I_{\rm C}$

Sample	Magnitude/Color Transformation			RMS residuals
	$ugriz$ to $UBVR_{\rm C}I_{\rm C}$			
Quasars at $z \leq 2.1$ (synthetic)	$U-B$	=	$0.75(u-g)-0.81$	0.03
	$B-V$	=	$0.62(g-r)+0.15$	0.07
	$V-R$	=	$0.38(r-i)+0.27$	0.09
	$R-I$	=	$0.72(r-i)+0.27$	0.06
	B	=	$g+0.17(u-g)+0.11$	0.03
	V	=	$g-0.52(g-r)-0.03$	0.05
Stars with $R-I<1.15$ and $U-B<0$	$U-B$	=	$0.77(u-g)-0.88$	0.04
	$B-V$	=	$0.90(g-r)+0.21$	0.03
	$V-R$	=	$0.96(r-i)+0.21$	0.02
	$R-I$	=	$1.02(r-i)+0.21$	0.01
	B	=	$g+0.33(g-r)+0.20$	0.02
	V	=	$g-0.58(g-r)-0.01$	0.02
All stars with $R-I<1.15$	$U-B$	=	$0.78(u-g)-0.88$	0.05
	$B-V$	=	$0.98(g-r)+0.22$	0.04
	$V-R$	=	$1.09(r-i)+0.22$	0.03
	$R-I$	=	$1.00(r-i)+0.21$	0.01
	B	=	$g+0.39(g-r)+0.21$	0.03
	V	=	$g-0.59(g-r)-0.01$	0.01
	$UBVR_{\rm C}I_{\rm C}$ to $ugriz$			
Quasars at $z \leq 2.1$ (synthetic)	$u-g$	=	$1.25(U-B)+1.02$	0.03
	$g-r$	=	$0.93(B-V)-0.06$	0.09
	$r-i$	=	$0.90(R-I)-0.20$	0.07
	$r-z$	=	$1.20(R-I)-0.20$	0.18
	g	=	$V+0.74(B-V)-0.07$	0.02
	r	=	$V-0.19(B-V)-0.02$	0.08
Stars with $R-I<1.15$ and $U-B<0$	$u-g$	=	$1.28(U-B)+1.14$	0.05
	$g-r$	=	$1.09(B-V)-0.23$	0.04
	$r-i$	=	$0.98(R-I)-0.22$	0.01
	$r-z$	=	$1.69(R-I)-0.42$	0.03
	g	=	$V+0.64(B-V)-0.13$	0.01

2.2. Photometric transformation for quasars

To account for the different spectral shapes of stars and quasars, in particular the presence of strong emission lines, we derive separate transformation equations for quasars. Since all quasars are variable at optical wavelengths, it would be necessary to use contemporaneous SDSS and *UB* photometry of a sample of quasars to derive adequate transformations from observations. As such observations are not available, we perform synthetic photometry of an updated version of the composite from Vanden Berk et al. (2001) using DR1 data (Abazajian et al. 2003; changes in spectrophotometric calibration of SDSS data introduced in DR2 do not change the transformations appreciably) and the composite spectra from Richards et al. (2003) for quasars with different intrinsic colors and reddening. We use the STSDAS Synphot package under the PyRAF scripting environment[3] and the Landolt filter curves provided with that package as well as the SDSS transmission curves[4] to determine color and magnitude differences for each composite. We compute a set of colors each at redshifts ranging from 0 to 2.1 in steps of 0.05 for the Vanden Berk et al. (2001) composite and 0.3 to 1.6 for the remaining composite spectra, which cover a smaller range of rest-frame wavelengths. For the comparison with BQS photometry, we fit $U-B$ and $B-g$ as a function of both $u-g$ and $g-r$ for all composites simultaneously. As both $U-B$ and $B-g$ are more tightly correlated with $u-g$ than with $g-r$, we use the fits as a function of $u-g$ to derive the transformations. The synthetic photometry results and best-fit lines are shown in Figure 2. The resulting coefficients are also given in Table 1, which again also contains transformations for the remaining SDSS and $UBVR_{\rm C}I_{\rm C}$ filters for reference.

The RMS scatter in the transformed quantities is 0.03, smaller than the plot suggests to the eye, although the $B-g$ residuals can be as large as 0.1 and show some systematic behavior with redshift. These systematics are caused by the presence of emission lines; the transformations as given have a precision of 0.06 or better in transforming pure power-law spectra. The $U-B$ transformation is only slightly different from that for blue stars, but the $B-g$ transformation differs significantly — not only do we fit $B-g$ as a function of $u-g$ instead of $g-r$, but even if we had used $g-r$, the transformations would differ by between 0.06 to 0.2 magnitudes in the $g-r$ range of quasars (-0.1 to 0.5). With the transformations in hand, we now consider the SDSS photometry of PG sources.

---

[3]Obtained from http://www.stsci.edu/resources/software_hardware/

[4]Available at http://www.sdss.org/dr2/instruments/imager/#filters

Table 1—Continued

Sample	Magnitude/Color Transformation			RMS residuals
	r	=	$V - 0.46(B-V) + 0.11$	0.03
All stars with $R-I < 1.15$	$u - g$	=	$1.28(U-B) + 1.13$	0.06
	$g - r$	=	$1.02(B-V) - 0.22$	0.04
	$r - i$	=	$0.91(R-I) - 0.20$	0.03
	$r - z$	=	$1.72(R-I) - 0.41$	0.03
	g	=	$V + 0.60(B-V) - 0.12$	0.02
	r	=	$V - 0.42(B-V) + 0.11$	0.03

Note. — Transformations for quasars are derived from synthetic photometry of an updated version of the quasar composite from Vanden Berk et al. (2001) using DR1 data as well as the red and reddened quasar composites from Richards et al. (2003). Transformations for stars are derived from $u'g'r'i'z'$ photometry (on the system of the USNO 1.0 m telescope) of Landolt standards given by Smith et al. (2002) after transformation to $ugriz$ (the system of the SDSS 2.5 m survey telescope) using the equations given by Gunn (2003). Smith et al. (2002) showed that stars with $R-I < 1.15$ have different color transformations than those with $ri \geq 1.15$; as there is no Landolt photometry of a sufficient number of SDSS standards with $R-I \geq 1.15$, we restrict ourselves to $R-I < 1.15$ here.

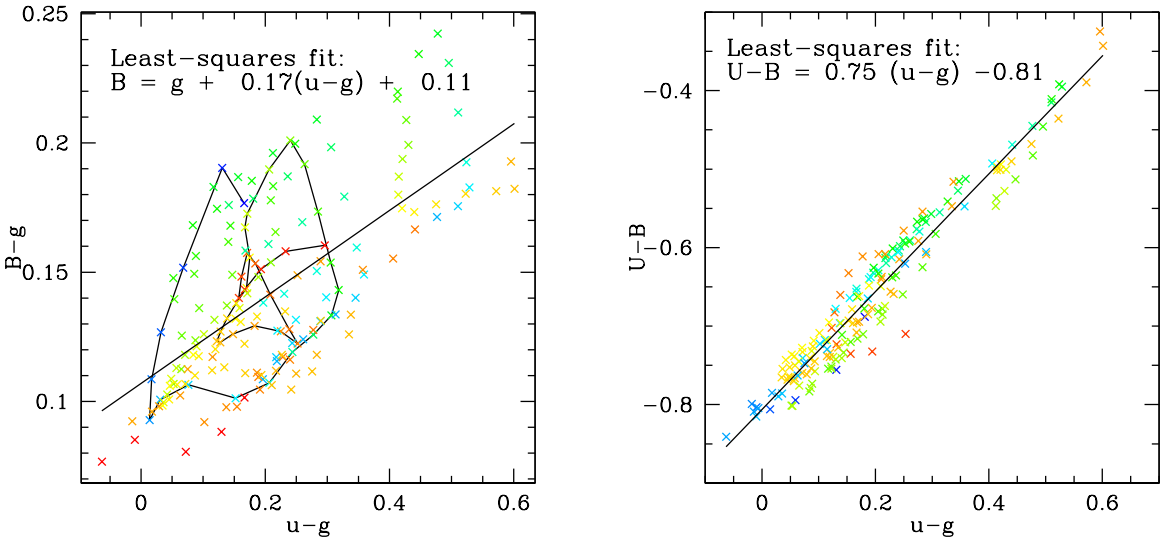

Fig. 2.— Transformation of quasar colors and magnitudes from SDSS *ug* to Landolt *UB* obtained from synthetic photometry of quasar composites at redshifts from 0 to 2.1 in steps of 0.05. Points are color-coded by redshift in the on-line edition. The points belonging to the updated version of the composite from Vanden Berk et al. (2001) are connected by a solid line in the left-hand plot to illustrate the change in color and magnitude difference as a quasar spectrum is redshifted; the remaining points are for the red and reddened composites from Richards et al. (2003). The diagonal solid lines show the best-fit straight line. The RMS scatter about the best fit is less than 0.03 in both cases.

2.3. SDSS observations of PG sources

We are interested in the SDSS photometry of PG sources, both to determine whether there are any systematics in the photometric calibration of the PG survey, and to compare the PG quasars to those selected by the SDSS quasar survey with its much wider color selection criteria and magnitude cut in a much longer-wavelength band. To this end, we cross-match the PG catalog with the SDSS DR3 data. The DR3 covers an area of 5282 square degrees; out of this area, roughly 3300 square degrees are contained within the PG area of 10,668 square degrees.

Because of the relatively large astrometric uncertainty of the PG survey (roughly $9''$ RMS in every coordinate with systematic offsets of less than $2''$; see §III in GSL86) and the different observing epochs, the closest SDSS object by position is not necessarily the correct match. We therefore use a generous positional matching radius of 2 arcminutes and employ cuts on the B magnitude and $U-B$ color transformed from SDSS photometry, accepting only objects within 1 magnitude of the PG photometry and with $U-B < -0.2$. This procedure results in up to 3 SDSS matches per PG object, of which we choose the object closest in $U-B$ color as the correct match. Every PG object has a counterpart detected in the SDSS. In our analysis below, we do not use photometry of matches which are saturated in the SDSS or have otherwise unreliable photometry using the flag checking recommendations for point sources from the SDSS web site[5]; this affected 9 objects.

We find 52 matches for BQS quasars in the DR3 photometric catalog which are shown in Table 2. All of these are either identified as quasar candidates by the SDSS target selection, have a cosmetic defect that excludes them from target selection (this affected 5 objects; the criteria for cosmetic defects are described in detail in Richards et al. 2002; Vanden Berk et al. 2005 estimate that the fraction of quasars missed due to image defects and blends is approximately 4%), or are brighter than the SDSS spectroscopic bright limit of $i > 15$ which has been introduced to avoid fiber cross-talk and saturation in the spectrograph. Thus, every BQS quasar is either targeted by the SDSS, or we understand why it was not targeted. However, even if target *selection* is complete, spectra of individual PG quasars may still be missing in the SDSS quasar survey if an object was not targeted by one of the pre-final versions of the target selection algorithm, or because of less reliable photometry in the TARGET version of photometry (see discussion of TARGET and BEST photometry in Abazajian et al. 2004a, §3). This affects one PG object for which DR3 photometry is available: the final quasar target selection algorithm correctly identified PG 1012+00 as a quasar candidate, but the TARGET version of the photometry does not recognize it as a quasar, merely

[5]http://www.sdss.org/dr3/products/catalogs/flags.html

as a counterpart to a ROSAT source. The quasar resides in a host galaxy with complex morphology (perhaps a merging system), with a bright galactic nucleus approximately $2''$ away from the quasar. The galactic nucleus was targeted as a galaxy and obtained a fiber (Plate/MJD/Fiberid 270/51909/586), while the quasar itself did not, because galaxy targets obtain a fiber with higher priority than ROSAT matches (see Stoughton et al. 2002; Blanton et al. 2003).

The photometric calibration is most easily addressed by considering only non-variable stars, which are also much more numerous than the PG quasars. We obtain 466 SDSS matches of PG stars (i.e., objects classified as white dwarf or hot subdwarf by SG83) with clean SDSS photometry in the DR3 area.

Table 2. Properties of BQS objects in the SDSS DR3 area

PG Name	RA[a] (J2000)	DEC (J2000)	u	g	r	B (PG)	B (SDSS)	$U-B$ (PG)	$U-B$ (SDSS)	Phot (1)	Targ (2)	Plt	MJD	Fib	z (SDSS)	z (BQS)
0003+15	00 05 59.24	16 09 49.01	15.66	15.38	15.48	15.96	15.54	−0.83	−0.61	1000	0011	···	···	···	···	0.450
0157+00	01 59 50.25	00 23 40.84	15.91	15.89	15.97	15.20	16.00	−0.26	−0.79	0000	0011	403	51871	550	0.163	0.164
0844+34	08 47 42.47	34 45 04.40	14.80	14.65	14.57	14.00	14.79	−0.75	−0.70	1000	1001	···	···	···	···	0.064
0921+52	09 25 12.85	52 17 10.50	16.72	16.35	16.19	15.62	16.53	−0.35	−0.54	0000	0011	767	52252	418	0.035	0.035
0934+01	09 37 01.05	01 05 43.71	16.72	16.61	16.54	16.29	16.74	···	−0.73	0010	0001	476	52314	523	0.051	0.050
0947+39	09 50 48.39	39 26 50.52	16.26	16.30	16.48	16.40	16.40	−0.50	−0.84	1000	0011	1277	52765	332	0.206	0.206
0953+41	09 56 52.39	41 15 22.25	14.99	14.93	14.95	15.05	15.05	−0.98	−0.76	1000	1001	···	···	···	···	0.239
1001+05	10 04 20.14	05 13 00.46	16.60	16.43	16.40	16.13	16.57	−0.52	−0.69	1000	0011	995	52731	4	0.160	0.161
1012+00	10 14 54.90	00 33 37.41	16.36	16.27	16.11	15.89	16.40	−0.44	−0.75	1000	0111	···	···	···	···	0.185
1022+51	10 25 31.28	51 40 34.88	16.27	16.11	16.04	16.12	16.25	−0.37	−0.69	0000	0011	1008	52707	558	0.045	0.045
1049−00	10 51 51.44	−00 51 17.66	16.00	15.80	15.70	15.95	15.95	−0.49	−0.66	1000	0011	276	51909	251	0.359	0.357
1103−00	11 06 31.77	−00 52 52.37	16.41	16.27	16.45	16.02	16.41	−0.40	−0.71	1000	0111	···	···	···	···	0.425
1114+44	11 17 06.40	44 13 33.31	16.01	15.89	15.79	16.05	16.02	−0.55	−0.72	1000	0011	1365	53062	378	0.144	0.144
1115+08	11 18 16.95	07 45 58.19	16.41	16.24	16.28	15.84	16.38	−0.52	−0.69	1000	0011	1617	53112	467	1.734	1.722
1115+40	11 18 30.29	40 25 54.01	15.83	15.91	16.00	16.02	16.01	−0.64	−0.87	1000	0111	1440	53084	204	0.155	0.154
1119+12	11 21 47.12	11 44 18.99	15.27	15.12	14.99	14.65	15.26	−0.57	−0.70	0000	1001	···	···	···	···	0.049
1121+42	11 24 39.18	42 01 45.02	16.14	15.99	15.94	16.02	16.12	−0.67	−0.70	1000	0011	1443	53055	358	0.225	0.234
1138+04	11 41 16.53	03 46 59.57	17.15	17.09	17.12	16.05	17.21	···	−0.77	1000	0011	838	52378	47	1.877	1.876
1148+54	11 51 20.46	54 37 33.08	15.84	15.72	15.57	15.82	15.85	−0.50	−0.72	1000	0111	1017	52706	187	0.975	0.969
1151+11	11 53 49.27	11 28 30.44	16.32	16.39	16.41	15.51	16.49	−0.57	−0.87	1000	0011	1610	53144	249	0.176	0.176
1206+45	12 08 58.01	45 40 35.47	15.67	15.47	15.24	15.79	15.61	−0.66	−0.66	1000	0011	1370	53090	360	1.164	1.158
1216+06	12 19 20.93	06 38 38.52	15.41	15.35	15.24	15.68	15.47	−0.42	−0.76	1110	0001	···	···	···	···	0.334
1226+02	12 29 06.70	02 03 08.59	12.72	12.80	12.73	12.86	12.90	−1.18	−0.87	1110	0001	···	···	···	···	0.158
1244+02	12 46 35.25	02 22 08.79	16.41	16.30	16.31	16.15	16.43	−0.49	−0.73	0000	0011	522	52024	173	0.048	0.048
1254+04	12 56 59.93	04 27 34.39	16.47	16.24	16.06	15.84	16.39	−0.40	−0.64	1000	0011	848	52669	154	1.025	1.024
1259+59	13 01 12.93	59 02 06.75	15.71	15.57	15.64	15.60	15.70	−0.70	−0.70	1000	0011	957	52398	20	0.477	0.472
1307+08	13 09 47.00	08 19 48.24	15.56	15.64	15.62	15.28	15.74	−0.82	−0.87	1000	0011	···	···	···	···	0.155
1322+65	13 23 49.52	65 41 48.17	16.18	16.16	16.12	15.86	16.27	···	−0.79	1000	0011	···	···	···	···	0.168
1329+41	13 31 41.13	41 01 58.70	16.99	17.06	17.11	16.30	17.16	−0.38	−0.86	1000	0011	1464	53091	433	1.938	1.930
1338+41	13 41 00.78	41 23 14.08	16.69	16.51	16.35	16.08	16.65	···	−0.67	1000	0011	1377	53050	338	1.215	1.219
1351+64	13 53 15.83	63 45 45.65	14.66	14.54	14.54	15.42	14.67	−0.53	−0.72	1000	1001	···	···	···	···	0.087
1352+01	13 54 58.68	00 52 10.89	16.23	16.07	15.92	16.03	16.21	−0.47	−0.69	1000	0011	···	···	···	···	1.117
1411+44	14 13 48.33	44 00 13.96	14.53	14.47	14.55	14.99	14.59	−0.81	−0.76	1110	0001	···	···	···	···	0.089
1415+45	14 17 00.82	44 56 06.36	16.67	16.53	16.32	15.74	16.66	−0.79	−0.70	0001	0001	1287	52728	296	0.114	0.114

2.3.1. SDSS observations of PG stars: the accuracy of the PG photographic magnitudes

Using the transformations established in §2.1, we derive the UB photometry of non-variable PG stars from their matches in SDSS data. GSL86 report a B-band magnitude (transformed to the standard Johnson system, which we assume to be identical to the Landolt system here) derived from the photographic photometry for every object in the survey, as well as a photoelectric B magnitude (which we will designate B_p) and $U-B$ color for a small subset of the stars. The photographic $U-B$ colors were not reported by GSL86 because they were deemed less reliable as indicator of each source's spectral type than the spectroscopic information. However, one of the authors (RG) retrieved archival notes with the photometric $U-B$ colors for most of the BQS objects (i.e., the quasars from the PG survey), we will compare those to SDSS photometry in §2.3.2 below.

GSL86 give an error of $\sigma_{B_p} = 0.05$ for the photoelectric magnitudes, comparable to the accuracy of the SDSS CCD photometry ($\sigma_u = 0.03, \sigma_g = 0.02$). Both of these measures are much more accurate than the photographic-plate derived magnitudes with their quoted error of $\sigma_B = 0.29$ (GSL86).

We begin with a comparison of the PG and SDSS magnitudes of these stars in Figure 3 (left-hand panels). We first compare the PG photoelectric B_p and the SDSS B magnitudes of the 104 stars in the overlap sample which also have photoelectric PG photometry. The mean difference of -0.03 is comparable to the photometric accuracy of the SDSS data. The observed RMS difference of 0.18 is much larger than the $\sigma_{B_p} = 0.05$ given by GSL86. However, after iterative rejection of 3σ outliers, the RMS difference drops to 0.075, as expected when considering the difference of two quantities where each has an error of 3%-5%. The different RMS is thus caused by a non-Gaussian error distribution in the PG photoelectric photometry. A similar comparison of photoelectric and SDSS $U-B$ shows a mean and median offset of 0.01 and a surprisingly small RMS difference of 6% (even without outlier rejection).

We next compare the photographic-plate derived B magnitudes to SDSS-derived B magnitudes for all non-variable PG stars matched in the SDSS, as well as to the PG photoelectric B_p, where available (right-hand panels in Figure 3). The comparison shows that there are systematic differences between the "low-accuracy" PG photographic magnitudes and both of the "high-accuracy" magnitudes, the SDSS B and the photoelectric B_p magnitudes. The PG photographic magnitudes are too bright by about 0.2 magnitudes on average at $B \approx 17$, and similarly too bright at $B \approx 13$. At $B \approx 15$, the photographic magnitudes agree with those from the SDSS, with a smooth transition from either extreme, although there is a much larger scatter at the bright end. The original photographic calibration approximated the photographic S-curve by a linear fit in the magnitude range $14 < B < 16$, consistent with the small calibration differences we find within this magnitude range and the larger dif-

Table 2—Continued

PG Name	RA[a] (J2000)	DEC (J2000)	u	g	r	B (PG)	B (SDSS)	$U-B$ (PG)	$U-B$ (SDSS)	Phot (1)	Targ (2)	Plt	MJD	Fib	z (SDSS)	z (BQS)
1426+01	14 29 06.57	01 17 06.09	14.36	14.45	14.61	15.05	14.54	−1.32	−0.88	1000	1001	···	···	···	···	0.086
1427+48	14 29 43.07	47 47 26.20	16.95	17.02	16.92	16.33	17.12	−0.43	−0.86	1000	0011	···	···	···	···	0.221
1440+35	14 42 07.47	35 26 22.97	15.10	15.00	14.97	15.00	15.13	−0.53	−0.73	1000	1001	···	···	···	···	0.077
1444+40	14 46 45.94	40 35 05.76	15.85	15.88	15.85	15.95	15.99	−0.58	−0.83	1000	0011	1397	53119	190	0.268	0.267
1501+10	15 04 01.20	10 26 15.76	14.27	14.24	14.22	15.09	14.36	−1.16	−0.79	1000	1001	···	···	···	···	0.036
1512+37	15 14 43.07	36 50 50.41	16.75	16.67	16.75	15.97	16.79	−0.46	−0.74	1000	0111	1353	53083	580	0.371	0.371
1522+10	15 24 24.53	09 58 29.12	15.97	15.93	15.74	15.74	16.04	−0.50	−0.78	1000	0011	···	···	···	···	1.321
1534+58	15 35 52.41	57 54 09.55	15.34	15.29	15.12	15.54	15.41	−0.54	−0.77	0000	0011	615	52347	108	0.030	0.030
1535+54	15 36 38.38	54 33 33.31	15.58	15.20	15.01	15.31	15.37	−0.51	−0.53	1000	1001	···	···	···	···	0.038
1538+47	15 39 34.80	47 35 31.31	16.55	16.08	16.05	16.01	16.27	···	−0.46	1010	0001	···	···	···	···	0.770
1543+48	15 45 30.24	48 46 09.07	16.56	16.44	16.44	16.05	16.57	−0.54	−0.72	1000	0111	812	52352	355	0.400	0.400
1552+08	15 54 44.58	08 22 21.45	16.19	15.94	15.80	16.02	16.09	−0.45	−0.62	1000	0011	···	···	···	···	0.119
1612+26	16 14 13.20	26 04 16.20	16.38	16.38	16.17	16.00	16.49	−0.69	−0.81	0000	0011	1393	52824	35	0.131	0.131
1630+37	16 32 01.12	37 37 50.01	16.13	16.03	15.93	15.96	16.15	−0.28	−0.73	1000	0011	1173	52790	198	1.476	1.471
1704+60	17 04 41.38	60 44 30.50	15.63	15.43	15.24	15.90	15.58	−0.42	−0.66	1000	0011	353	51703	377	0.372	0.371
2130+09	21 32 27.82	10 08 19.16	14.73	14.70	14.80	14.62	14.81	···	−0.79	1000	1001	···	···	···	···	0.061
2214+13	22 17 12.26	14 14 20.89	14.55	14.51	14.50	14.98	14.62	···	−0.78	1000	1001	···	···	···	···	0.067
2233+13	22 36 07.68	13 43 55.32	16.30	16.28	16.28	16.04	16.39	−0.62	−0.80	1000	0011	739	52520	388	0.326	0.325

[a]Unless indicated otherwise, all quantities are taken from the SDSS photometric and spectroscopic catalogs.

Note. — We use PG object names, B (PG) and z (BQS) for the BQS objects (Schmidt & Green 1983) as listed in the on-line tables from Kellermann et al. (1994, CDS VizieR catalog J/AJ/108/1163), which includes the corrections to the BQS catalog given by Green et al. (1986). The previously unpublished photographic $U-B$ colors from Schmidt & Green (1983) are given in column $U-B$ (PG) when available. B (SDSS) and $U-B$ (SDSS) have been obtained from SDSS u and g using the transformations given in §2.2. The columns *Phot* and *Targ* are sets of flags which give additional information about SDSS photometry and target selection in the `BEST` version of the photometric catalogs. (1) *Phot* contains information (in this order) on whether the source was a point source, saturated in any of the SDSS bands, had a fatal cosmetic error in quasar target selection, and whether it had a nonfatal cosmetic error in quasar target selection. (2) *Targ* contains information on whether the object was flagged as quasar candidate by color selection but is too bright to be observed with the spectrograph, targeted as FIRST source, targeted by color selection, and finally a "completeness" flag. This "completeness" flag is the logical OR of the flags indicating a fatal or non-fatal cosmetic error, of those identifying the object as color- or FIRST-selected target, and of the flag indicating a color-selected target that is too bright for inclusion in the spectroscopic survey. The "completeness" flag would be 0 if an object had neither been recognized as quasar target nor rejected only due to cosmetic problems, causing the object to be missed by SDSS target selection; it is 1 for all objects in the table, indicating that every BQS quasars was either targeted, or we understand why it was not targeted. The columns Plt, MJD, Fib give the plate/MJD/fiber combination identifying the SDSS spectrum, where available. All spectra of BQS objects were classified as quasar by the automated pipeline, with the redshift given as z (SDSS).

ferences outside it. There are no discernible systematic trends of this calibration difference with the $U-B$ color. This calibration difference changes not only the magnitudes of the PG objects (and hence the limiting magnitudes), but also the inferred scatter between the PG and other photometry. We therefore wish to recalibrate the PG B magnitudes using SDSS and/or PG B_p photometry.

This recalibration *cannot* be done simply by fitting the PG photographic B magnitudes as function of the high-accuracy SDSS B and PG B_p magnitudes because the machine used to digitize the photographic plates did not report measurements of any objects fainter than the plate limit (which varied from plate to plate). Therefore, the points shown in the right two panels in Figure 3 are restricted to lie below the line $B = B_{\rm lim}$ for each PG plate (the dotted line shows the average $B_{\rm lim}$ of 16.16). Hence, no PG data are available for those objects which have been scattered out of the PG sample, and the fit is biased towards artificially bright B values at the faint end.

To allow a correction of the limiting magnitudes of each PG field, we instead perform a fit of the inverse relation, i.e. the SDSS or B_p magnitude as function of PG photographic magnitude. In this case, the censoring is applied in the independent variable, resulting in a less biased fit, provided that errors in both coordinates are taken into account. We obtain the following fit:

$$\begin{aligned} B &= 15.1364 + 0.9584\,(B_{\rm PG} - 15) \\ &\quad -0.1605\,(B_{\rm PG} - 15)^2 - 0.0160\,(B_{\rm PG} - 15)^3 \end{aligned} \qquad (1)$$

where $B_{\rm PG}$ designates the photographic PG magnitude. This fit is shown as green dashed line in Figure 3. This fit closely follows a non-parametric fit obtained by determining the median photographic magnitude as function of the high-precision magnitudes in bins of size $\Delta B = 0.1$.

We expect this calibration difference to be responsible for some of the scatter between photographic and other B magnitudes, so that the error of $\sigma_B = 0.29$ should be an overestimate of the actual error. However, the residuals of the corrected photographic B do not have a distribution that is appreciably narrower than the original residuals; in fact, both the original and the corrected residuals have an RMS of 0.34. Nevertheless, use of the fit clearly reduces the systematic calibration errors.

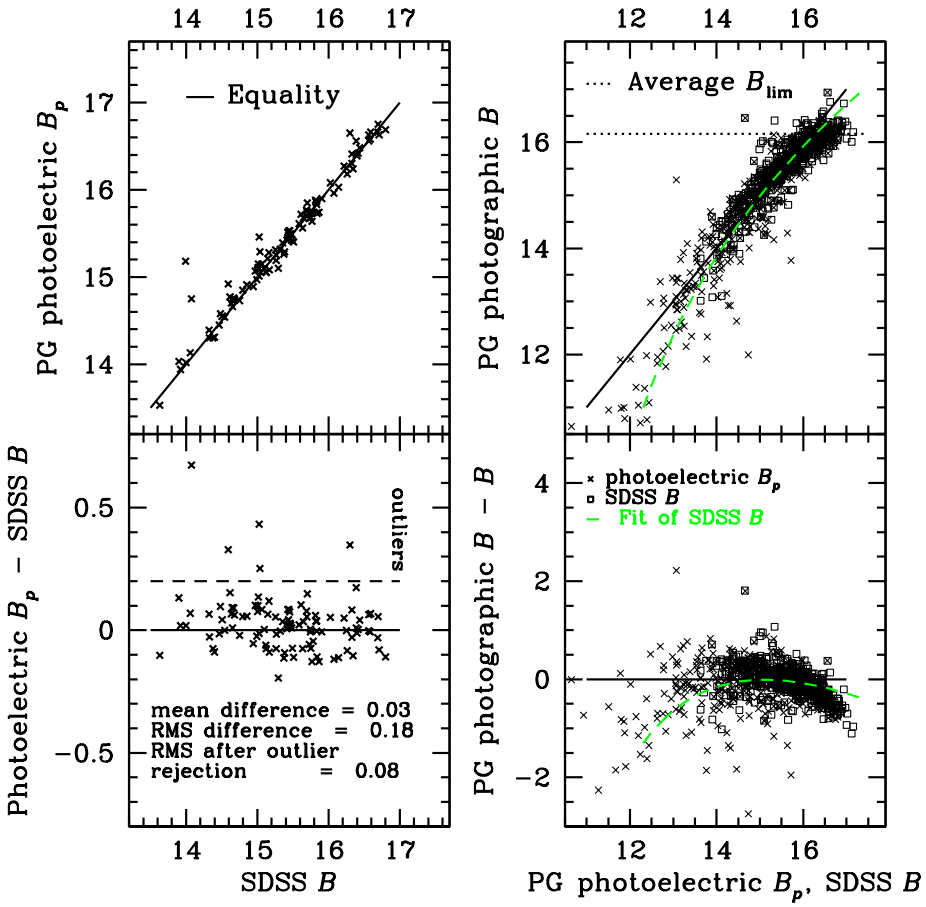

Fig. 3.— Comparison of SDSS and PG photometry for non-variable stars. *Left*, comparison of SDSS B to PG photoelectric B_p of 104 stars. *Right*, crosses show PG photoelectric B_p, squares show SDSS B against PG photometric B derived from photographic plates. In both cases, the upper panel shows the direct comparison of the magnitudes with the solid diagonal line indicating equality, while the lower panel shows the difference as a function of the more accurate magnitude. The dashed green lines in the right-hand side panels show the best-fit cubic (Equation 1) describing the SDSS-derived or PG photoelectric B magnitudes as function of the PG photographic B magnitude. This fit adequately describes the calibration difference between PG photographic photometry and the Landolt system, while the more intuitive fit of the PG photographic magnitude as function of the PG photoelectric and SDSS B magnitudes (not shown) is biased towards fainter photographic B magnitudes by the removal of objects with photographic magnitudes fainter than the PG plate limits (the horizontal dotted line in the upper right-hand panel shows the effective limiting magnitude of 16.16).

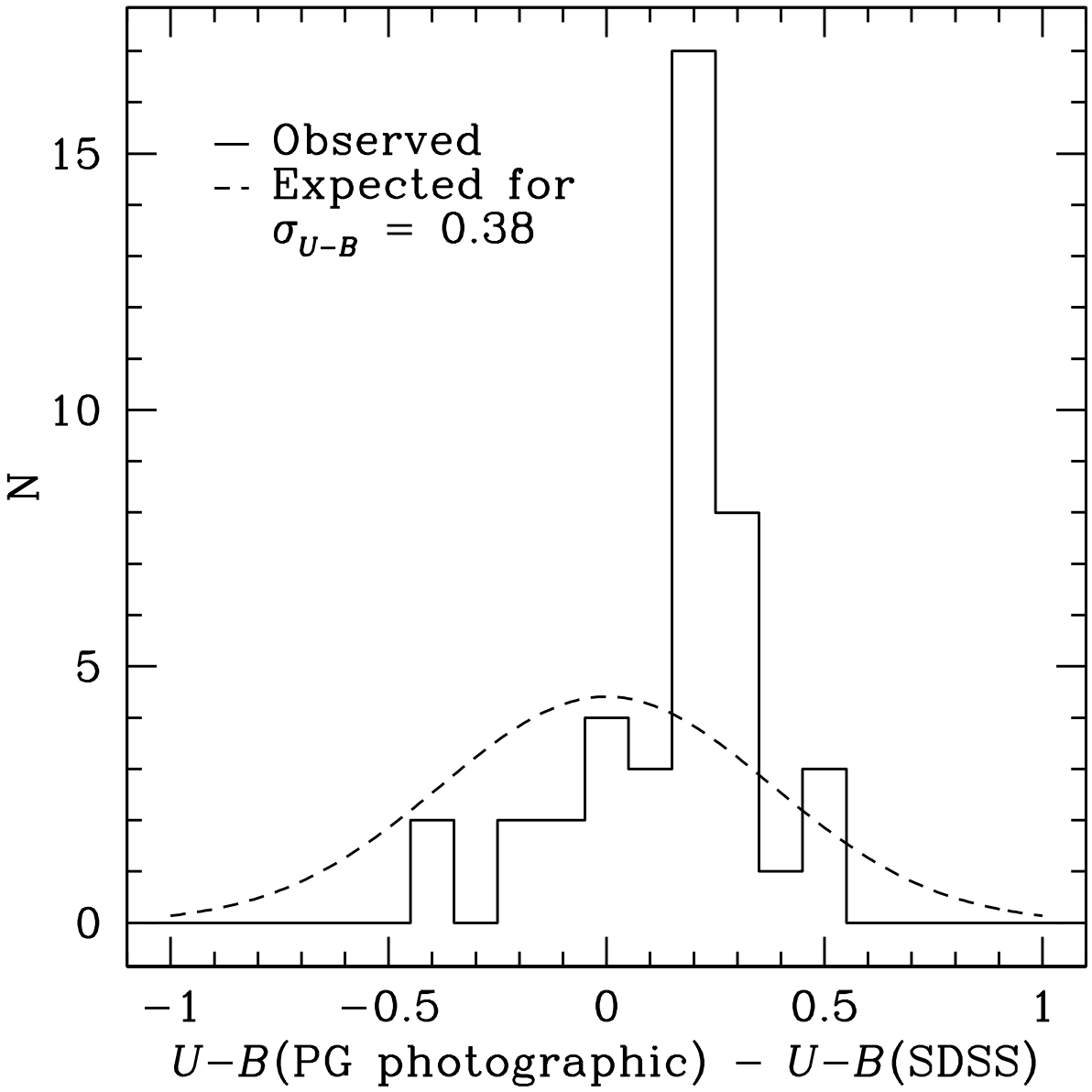

Fig. 4.— Distribution of the difference between $U-B$ colors of BQS objects derived from SDSS and PG photometry. The difference histogram is sharply peaked at $\Delta U-B = 0.2$, with a median difference of 0.19 and an RMS of 0.21. The dashed Gaussian indicates the expected difference histogram for the $U-B$ error of 0.38 quoted by GSL86.

2.3.2. SDSS observations of BQS quasars: the accuracy of the PG photographic colors and B-band variability

We now turn to the comparison of SDSS and PG $U-B$ colors, where the latter are available. Figure 4 shows the distribution of the difference between SDSS and PG-derived $U-B$ for the 47 BQS objects for which clean SDSS photometry is available. The distribution of residuals is sharply peaked at $\Delta(U-B) = (U-B)_{\rm PG} - (U-B)_{\rm SDSS} = 0.2$, with tails to ± 0.5. The RMS $U-B$ difference is 0.21 and is dominated by photometric errors. (Since the PG magnitude measurements are based on double exposures of the same plate, the PG U and B measurements are effectively contemporaneous, as are the SDSS observations in u and g.)

GSL86 only performed photoelectric photometry of non-variable stars, but not of any BQS objects; however, any color variability over the epoch difference between PG and SDSS will be negligible compared to the PG photographic color error (Vanden Berk et al. 2004), so that the color comparison is not affected by variability. Thus, judging from the peak in the $U-B$ difference histogram, the PG-recorded photographic $U-B$ colors are too red by about 0.2 magnitudes. As a consequence, we expect that the true color cutoff of the objects in the PG survey is in fact about 0.2 magnitudes *bluer* than assumed.

We compare SDSS and photographic B magnitudes of the quasars in our overlap sample in Figure 5. On average, the quasars are fainter by 0.4 magnitudes at the SDSS epoch, with an RMS difference of 0.54 magnitudes. Given an RMS difference σ, the expected magnitude offset is σ^2 times the logarithmic slope of the number-magnitude counts, or about $2\sigma^2$. Thus, the expected offset is about 0.5 magnitudes, consistent with the variability amplitude of 0.3 magnitudes expected over the approximately 30-year epoch difference between SDSS and PG observations (Helfand et al. 2001). The variability amplitude found here also agrees roughly with the structure function for quasars presented by de Vries et al. (2003).

In conclusion, we have found two key differences between the PG photographic photometry on the one hand, on which the PG color and magnitude selection is based, and SDSS and PG photoelectric photometry on the other hand: there is an offset between the PG photographic and the true B-band magnitudes which varies systematically with magnitude, as well as an offset of 0.2 magnitudes between the photographic and true $U-B$ color (objects appear redder in the PG survey than they are), for which no systematic variation with magnitude could be established. To double-check the validity of these conclusions, we now simulate the PG survey's selection of objects from its parent sample as observed with the SDSS.

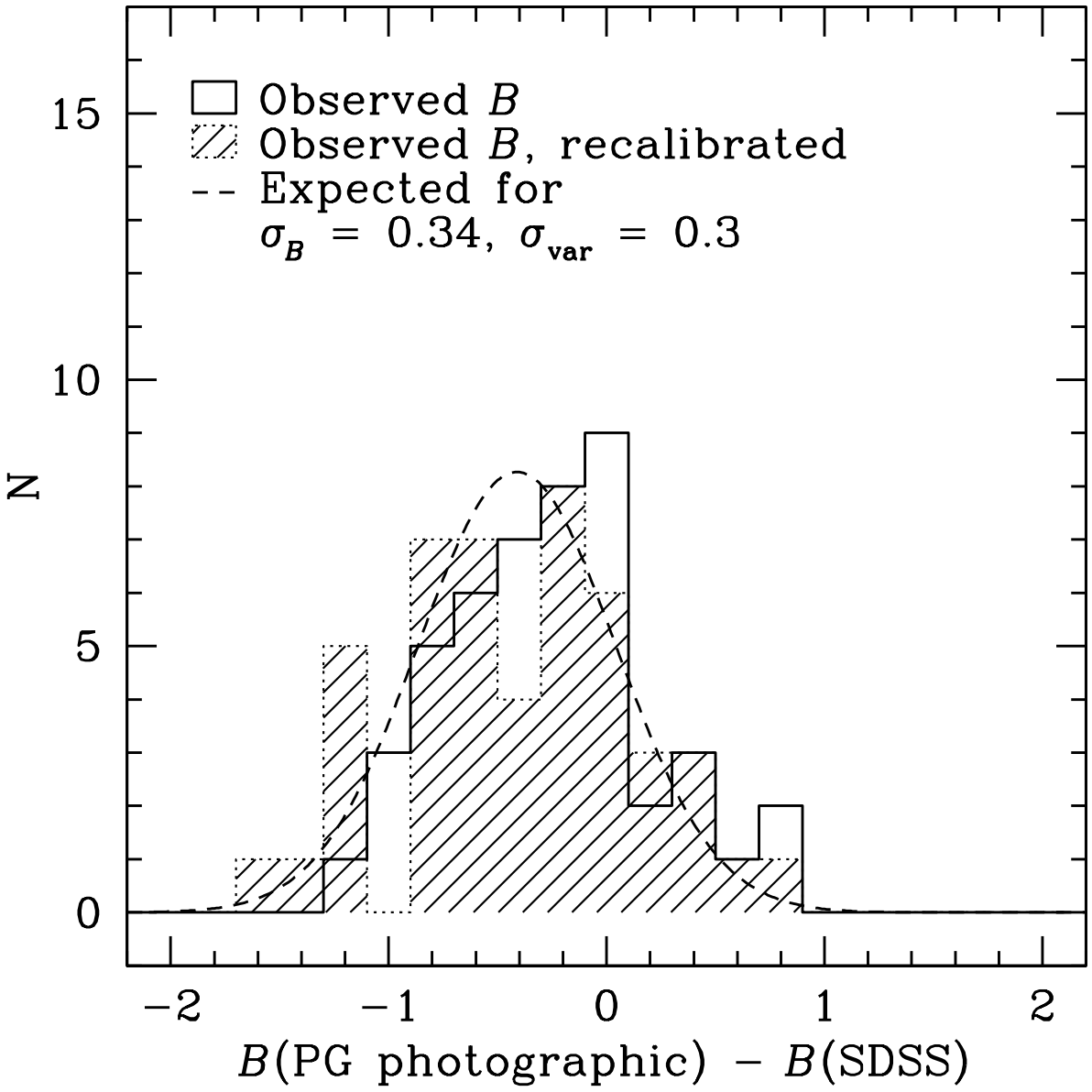

Fig. 5.— Distribution of the difference between B magnitudes of BQS objects derived from SDSS and PG photometry. The unshaded histogram shows the distribution of differences between SDSS and PG photographic B magnitudes as reported by SG83, while the shaded histogram shows the distribution of differences after correcting the PG photographic magnitudes using the fit derived above (Equation 1). The recalibrated magnitudes have a mean offset of B(SDSS) − B(PG) = −0.40, and a median offset of −0.32. The RMS difference is 0.54 magnitudes. Both offset and RMS appear reasonably consistent with the offset anticipated for an RMS quasar variability of 0.3 magnitudes over the 30-year epoch difference between SDSS and PG, as indicated by the dashed Gaussian curve.

3. Completeness of the PG sample relative to UV excess sources from the SDSS

We quantify the PG sample incompleteness by selecting SDSS object that pass the PG photometric selection criteria. Inclusion in the PG catalog of UV excess objects furthermore required that objects pass a spectroscopic confirmation as off-main sequence object or quasar. This process led to the exclusion of 1125 main-sequence objects that had been scattered into the photometric sample. SDSS spectroscopic target selection explicitly rejects objects with the colors of white dwarfs to improve the selection efficiency of quasar candidates (Richards et al. 2002), so that a similar spectroscopic confirmation is not available for objects passing the PG criteria in SDSS photometry. However, the photometric calibration of the SDSS is sufficiently accurate to allow a clean separation of main-sequence and PG-like UV excess objects in the $U-B$ against B color-magnitude diagram. Essentially all objects with $U-B < -0.3$ that are not saturated in SDSS photometry are off the main sequence (the magnitude at which objects are saturated of course depends on the seeing; the brightest unsaturated object has a PSF magnitude $r = 12.1$, and objects as faint as $r = 14$ can contain saturated pixels).

From this parent sample, we can directly simulate the expected color and magnitude distribution of objects in the PG sample, in the following manner. Using the positions of the plate centers and limiting magnitudes from Table 1 in GSL86, we determine in which PG survey plates each SDSS object is contained (for simplicity, we approximate the shape of PG survey plates as perfect circles of area 59.14 square degrees, i.e., with radius $4\overset{\circ}{.}33876$) and note the faintest applicable PG limiting magnitude in areas covered by multiple plates with different limiting magnitudes. We transform SDSS magnitudes into the *UB* system using the transformations derived above (we apply the quasar transformations from §2.2 to those objects with a quasar spectrum in the SDSS, and the stellar transformations §2.1 for all others). For every SDSS object, we also determine whether it has been included in the PG catalog. In this way, we can compare the completeness of the PG survey *relative* to the SDSS; i.e., we can determine whether there are any color or magnitude systematics to the incompleteness. We are not making any statements about the *absolute* surface density of UV excess objects in this section.

Figure 6 shows the color-magnitude diagram of our SDSS parent sample, defined as all objects with $U-B < -0.3$ and $B < 17.6$ ($3\ \sigma_B$ fainter than the faintest PG plate limit). We account for the calibration difference between PG and SDSS B magnitudes by recalibrating the PG limiting magnitudes using the transformation from PG to SDSS magnitudes derived above (Equation 1). We then calculate the PG detection probability for each object in our parent sample from the values of the limiting magnitude of each plate, the $U-B$ cut, and the

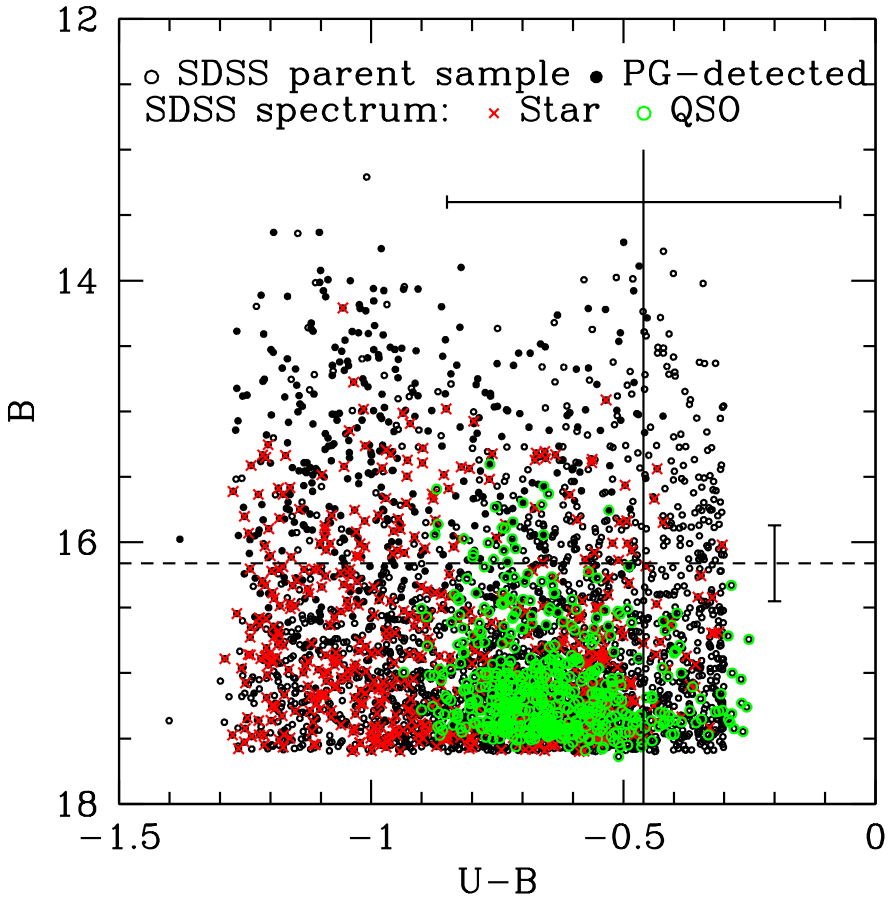

Fig. 6.— Color-magnitude diagram showing the parent sample of the PG survey of UV excess objects selected from SDSS photometry. We show all SDSS objects with clean photometry, $U-B < -0.3$ and $B < 17.6$ located within a PG survey plate (i.e., less than 4.°33876 from a plate center). Filled circles represent objects with PG detections. Colored symbols indicate SDSS spectroscopic classification where an SDSS spectrum is available: red crosses for stars (predominantly white dwarfs and hot subdwarfs) and green circles for quasars. The vertical solid line and the associated error bar indicate the nominal PG color cut of -0.46 (-0.44 for quasars) and the error on the $U-B$ photographic color, while the dashed horizontal line and its error bar show the average limiting B magnitude of 16.16 and the photographic B magnitude error. All objects were selected from SDSS photometry assuming the photometric transformations for stars from §2.1. All objects were *selected* from SDSS photometry assuming the photometric transformations for stars (§2.2), although the spectroscopically confirmed quasars are *plotted* here using the quasar transformations; the resulting color difference of at most 0.1 accounts for the few quasars appearing redder than $U-B = -0.3$.

respective PG photometric errors, assuming a Gaussian error distribution. By summing the detection probabilities for all objects in a given color or magnitude bin, we directly obtain the expected color and magnitude distributions for the PG survey.

Figure 7 shows the predicted distributions for B magnitude, $U-B$ color, and detection probability (dotted red histograms) and compares them to the distributions as observed in the PG (black histograms). The SDSS observations and the color cut and photographic errors as given by GSL86 lead to an overprediction of the number of PG objects with colors close to the $U-B < -0.46$ cutoff and with magnitudes in the range $15 < B < 16.5$, i.e., within a magnitude or so of the average limiting B magnitude. These "missing" objects have PG detection probabilities near 50% based on SDSS photometry. With hindsight, Figure 6 already reveals that the PG is missing objects with $U-B$ colors close to the cutoff: for a Gaussian error distribution, the detection probability of an object close to the color cut is close to 50%, but PG detections nearly exclusively lie to the blue of the nominal color cut of -0.46. To reduce the number of red objects in the simulated PG and to match the slope of the $U-B$ histogram's cutoff towards redder $U-B$ colors, it is necessary to adjust the color cut to $U-B = -0.71$ and the $U-B$ error to $\sigma_{U-B} = 0.24$ (as originally quoted by SG83), resulting in the cyan shaded histograms shown in Figure 7. The offset between the corrected $U-B$ cut and the value we find is comparable to the offset of about 0.2 magnitudes between SDSS and PG $U-B$ colors of quasars we determined above (§2.3.2 and Figure 4).

There is a related test based on the number of main-sequence objects scattered into the photometric sample. At a given B magnitude, the number of objects per unit $U-B$ color increases sharply into the main sequence, redwards of $U-B = -0.3$. Therefore, the number of main-sequence objects that are scattered into the PG photometric sample and subsequently need to be removed in the spectroscopic confirmation process is extremely sensitive to changes in the $U-B$ cut and error. We repeat the detection probability calculation for objects with $-0.3 < U-B < 0$ to obtain a lower limit on the average number of main-sequence objects we expect to be scattered into the photometric sample for a given combination of color and magnitude cuts and errors. We obtain a prediction of more than 17,000 main-sequence objects being scattered into the PG photometric sample for $U-B < -0.44$ and $\sigma_{U-B} = 0.38$, while the prediction for the revised values $U-B < -0.71$ and $\sigma_{U-B} = 0.24$ is roughly 500. These values are for the DR3-PG overlap area of roughly 3300 square degrees. The actual number of rejected main-sequence objects in the PG survey was 1125 over 10,668 square degrees, corresponding to roughly 300 over the overlap area considered here, and consistent with our revised color cut and photometric error. This finding is confirmed independently by a comparison of the sample of DA white dwarfs from the PG to samples selected in other wavebands, which shows color incompleteness beginning at $U-B = -1$ and increasing towards redder colors (Liebert et al. 2004, and Liebert, *priv. comm.*). This color

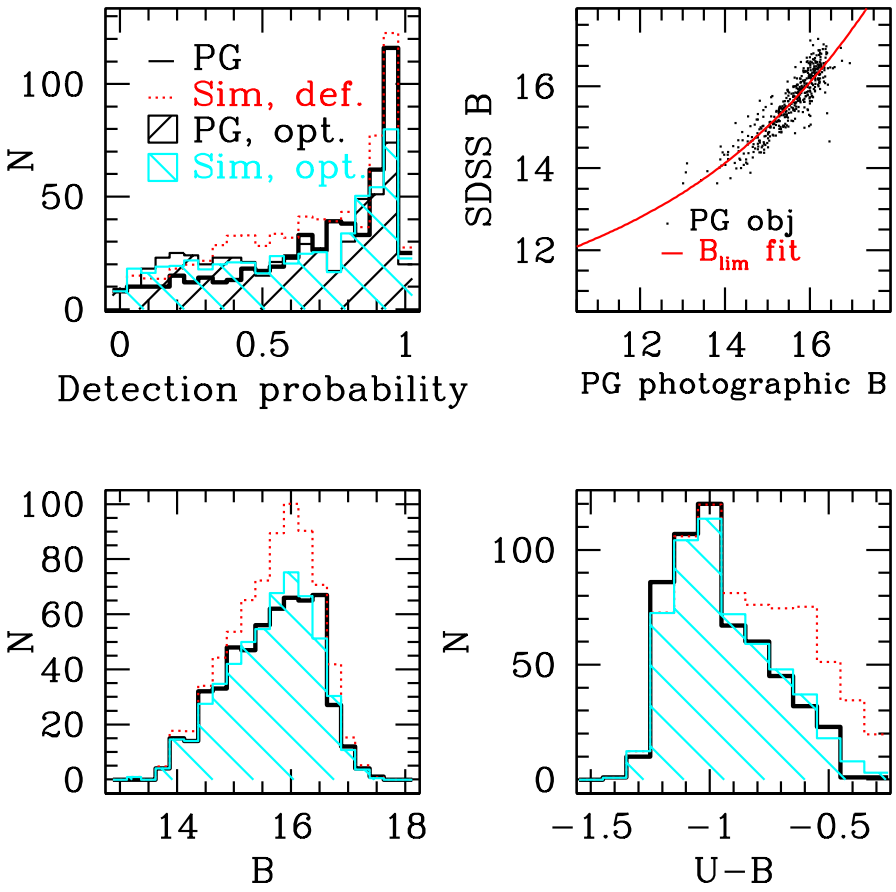

Fig. 7.— Comparison of parameter distributions from actual PG and SDSS-simulated PG survey. We calculate a detection probability in the PG survey for every SDSS object in Figure 6, based on the object's magnitude and color, each PG plate's limiting magnitude after recalibration using the fit from Equation 1 as shown in the upper right-hand panel, and two sets of limiting $U-B$, color and magnitude errors: a "default" set with parameters $\sigma_B = 0.34, \sigma_{U-B} = 0.36, (U-B)_{\rm lim} = -0.46$ as given by GSL86 (thick solid and dotted red histograms) and an "optimal" set $\sigma_B = 0.34, \sigma_{U-B} = 0.24, (U-B)_{\rm lim} = -0.71$ giving much better agreement between the observed and simulated distributions (black and cyan shaded histograms). With the errors and color cut as given by GSL86, the PG survey as simulated from the SDSS parent sample has many more objects with colors in the range $-1 < U-B < -0.3$ and with apparent magnitudes in the range $15 < B < 16.5$ than the actual PG survey. To reduce the number of red objects in the simulated PG and to match the slope of the $U-B$ histogram's cutoff towards redder $U-B$ colors, it is necessary to adjust the color cut to $U-B = -0.71$ and the $U-B$ error to $\sigma_{U-B} = 0.24$ (as originally quoted by SG83).

incompleteness is likely caused by the visual inspection process of the measurement-machine selected UV excess candidates, which cut down the number of candidates by a factor of 20 by removing objects that appeared to have a neutral $U-B$ color on the photographic plates.

In summary, we find that the PG survey had an effective color cut $U-B < -0.71 \pm 0.24$. We now consider how different the BQS quasar sample is from the BQS-like part of the SDSS quasar sample.

4. Comparison of PG quasars to SDSS quasars

The SDSS quasar survey reaches both to much fainter magnitude limits and samples a larger portion of non-stellar color space than the BQS. Our comparison of these two quasar surveys has two aims:

1. To consider whether the BQS has any systematic incompleteness. To address this question, we compare the BQS quasars to those DR3 quasars passing the nominal PG criteria $B < 16.16$ and $U-B < -0.44$ (we discuss this choice in detail in §4.1 below.)

2. To consider the impact of the BQS selection criteria themselves, i.e., determine the selection effects present in the BQS. To address this question, we consider which part of the entire DR3 quasar catalog is selected by the BQS criteria.

In order to obtain a meaningful comparison, we need to apply some cuts to obtain comparable samples. First, SDSS quasar spectroscopic target selection has a bright limit of $i > 15$ to avoid fiber cross-talk and saturation in the spectrograph. We therefore apply the same bright limit to SDSS matches of BQS quasars, leaving 39 BQS matches in the PG-DR3 overlap area of approximately 3300 square degrees. Furthermore, we restrict the SDSS spectroscopically identified quasars to $z < 2.2$ quasars selected using the *ugri* algorithm with faint limiting magnitude $i < 19.1$, since the *griz* algorithm is explicitly aimed at recovering quasars at $z > 2.2$ to which the BQS UV excess cut is insensitive. The resulting sample consists of 30,975 quasars, drawn from a subset of the DR3 area totaling 4188 square degrees.

4.1. Comparison of optical properties

4.1.1. Selection of a BQS-like set of quasars from the SDSS quasar sample

Even though we established above (§3) that the PG actually has an effective color cut $U-B < -0.71$, we select a "BQS-like" sample of SDSS quasars using the the intended limit

$U-B < -0.44$ because this is the value assumed by all previous comparisons of other quasar surveys to the BQS. Of the 30,975 SDSS quasars remaining in the comparison sample, 26 satisfy the nominal BQS criteria $U-B < -0.44$ and $B < B_{\rm eff} = 16.16$.

Furthermore, an object-by-object comparison between the BQS and BQS-like SDSS quasars is not particularly meaningful. First, the large photometric errors of the PG survey and the flux variability of quasars mean that a reobservation of the PG area using the same technology would not recover exactly the same set of objects. The BQS quasars in the range $15.4 < B < 17.2$ only have an average detection probability of 50%. Conversely, the average detection probability of SDSS quasars within 3σ of the intended PG cuts is less than 10%. Variability on average decreases the re-detection probability even further because quasars from a flux-limited sample on average become fainter. Secondly, the limiting magnitudes of the PG survey plates vary substantially (see Figure 1), and the surface density of bright quasars is very low (most PG fields contribute 0 or 1 quasars to the BQS). Therefore, a comparison of the full BQS to a survey with a different set of limiting magnitudes will be expected to result in many non-detections of BQS objects, and detections of non-BQS objects.

Hence, we prefer to compare the two surveys in a statistical sense, by analyzing the distribution of BQS and BQS-like quasars in redshift, magnitude and color space. We consider each of the two-dimensional projections of this three-dimensional parameter space in turn. Using matches between the FIRST radio survey (Becker et al. 1995) and SDSS data, we also consider the radio properties.

4.1.2. Magnitudes and colors as function of redshift

It is instructive for the understanding of selection effects to compare the properties of BQS quasars as well as BQS-like SDSS quasars to the entire set of SDSS quasars. We begin with the Hubble diagram, the apparent magnitude plotted against redshift, in Figure 8. Note that the number of bright objects decreases with increasing redshift. As expected from the larger magnitude errors and the limiting magnitude varying from plate to plate, the BQS quasars show some scatter about the effective limiting magnitude $B_{\rm eff}$, while the BQS-like SDSS quasars have a sharp magnitude cutoff. Other than that, the BQS and the BQS-like quasars have a similar distribution in the Hubble diagram.

Next, we consider the distribution of quasar colors against redshift shown in Figure 9. As noted before by several authors (e.g. Wisotzki et al. 2000; Richards et al. 2001, and references therein), there is a systematic variation of the $U-B$ color of quasars as a function

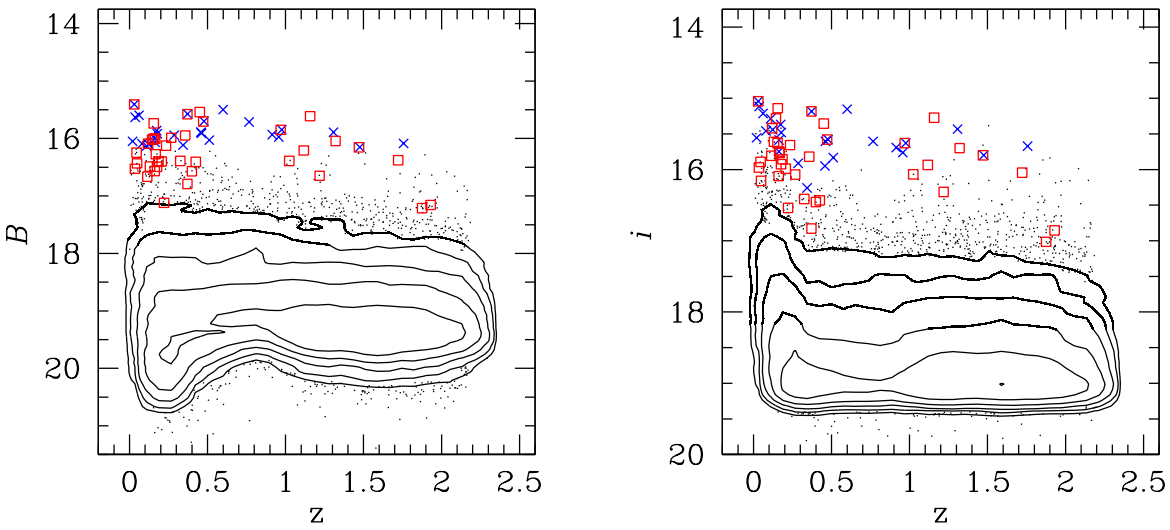

Fig. 8.— Hubble diagrams of SDSS DR3 *ugri*-selected quasars at $z < 2.2$ (dots and logarithmic contours increasing by a factor of 2), subset of DR3 quasars passing BQS criteria (crosses, blue in online edition), and BQS quasars in the DR3 area at $i > 15$ (open squares, red in online edition). Left, B-band; right, i-band. The B-band diagram shows that the density of B-bright objects declines towards higher redshifts. The overdensity of bright i-band quasars at $z < 0.3$ is a selection effect caused by the presence of the Hα line in the i-band filters at these redshifts. This also causes the corresponding overdensity of faint objects in the B-band diagram.

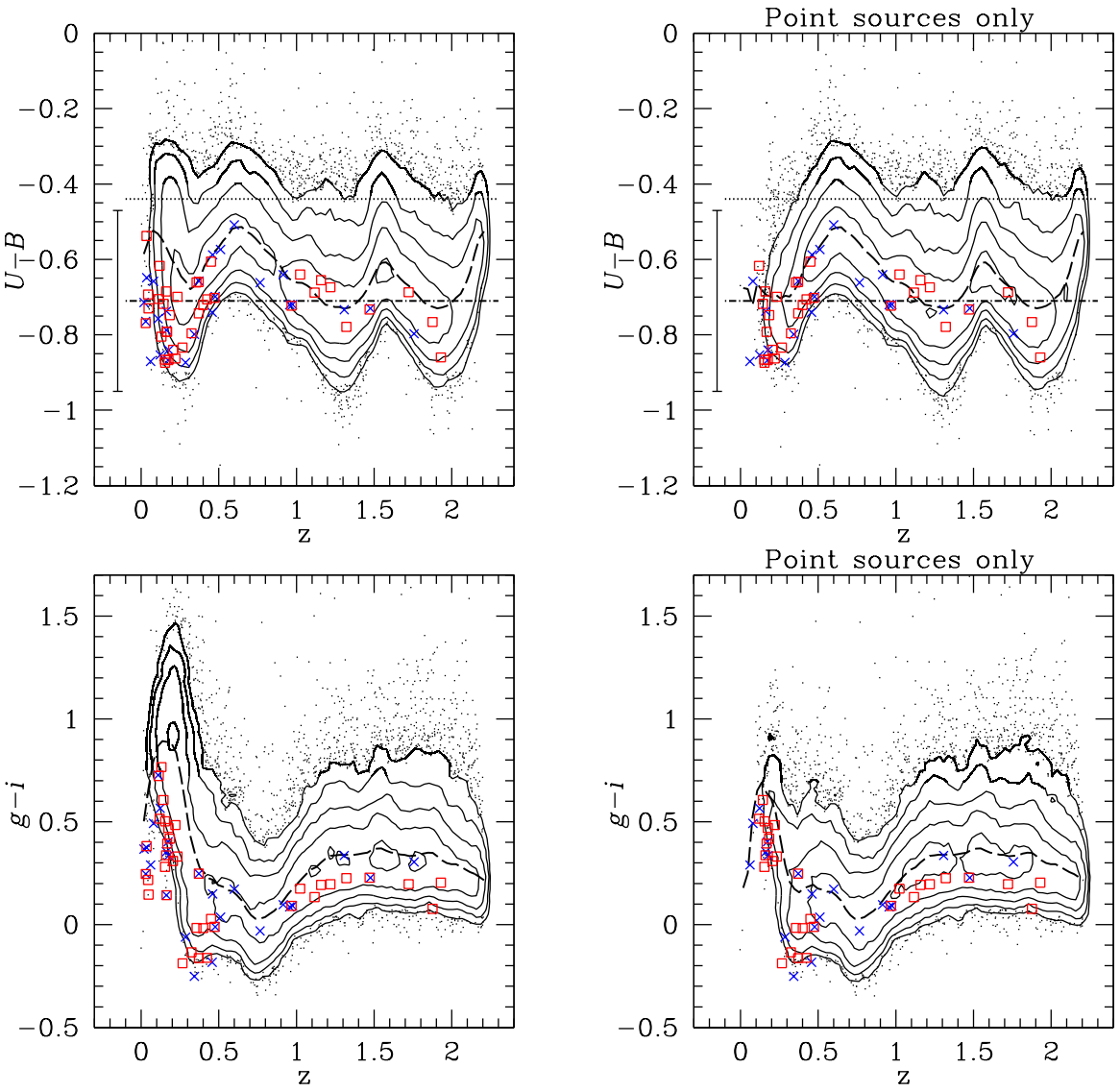

Fig. 9.— Colors of quasars as function of redshift. Above, $U-B$; below, $g-i$. Left column, all SDSS *ugri*-selected quasars at $z < 19.1$. Right column, excluding sources which are extended in SDSS photometry. Symbols as in other figures. The long-dashed line shows the median color in redshift bins of 0.01. The dotted line shows the nominal BQS color cut $U-B < -0.44$, while the dot-dashed line shows the actual color cut $U-B < -0.71$ with the error bar indicating the BQS $U-B$ error $\sigma_{U-B} = 0.24$ (see Figure 7).

of redshift, caused by emission lines passing into and out of the two filters. As discussed in detail by Wampler & Ponz (1985), application of a UV excess criterion in conjunction with this variation may lead to an observed redshift distribution that is not representative of the true redshift distribution. But again, the distributions of both $u-g$ and $g-i$ against redshift are very similar between the BQS and BQS-like SDSS quasars.

In addition to the emission-line effect described here, quasar colors can be reddened by the presence of host galaxy starlight, especially at low luminosity (and therefore low redshift), where the host galaxy is apparent in SDSS imaging. Indeed, excluding extended quasars from the color-redshift distribution (right-hand panels in Figure 9) bluens the median $U-B$ color at $z = 0.2$ by 0.2 magnitudes; the median $g-i$ colors are affected even more strongly. However, the BQS quasars are so luminous that the vast majority appear as point sources in SDSS imaging; thus it would be incorrect to compare colors of BQS quasars and the bulk of the SDSS quasars at the same redshift. Rather, we simply compare the *observed* $U-B$ and $g-i$ colors of BQS and BQS-like SDSS quasars at each redshift.

In conclusion, the colors and magnitudes of quasars as function of redshift are affected by the presence of emission lines and host galaxy starlight. These effects must be taken into account in the analysis of redshift, magnitude and color distributions of quasars, such as in the construction and interpretation of quasar luminosity functions.

4.1.3. Color-magnitude diagrams

Figure 10 shows the color-magnitude diagrams (CMDs) of the quasars at $z < 2.2$ from the DR3 spectroscopic quasar sample and the BQS quasars reobserved with the SDSS. The SDSS sample is flux-limited in i-band, as can be seen in the right-hand panel. The skewed cutoff to the B against $U-B$ distribution is caused by a combination of two effects: one is that the Hα line passes through the i-band at low redshifts, boosting quasars that are faint in B above the i-band flux limit. The other effect is the increased importance of red host-galaxy starlight for lower-luminosity quasars we mentioned above. Hence, quasars which are faint in B are also red in $U-B$.

The CMD shows clearly that the multicolor-selected SDSS quasars which are sufficiently bright to pass the BQS limiting magnitude in the B-band have a similar $U-B$ color distribution to the BQS quasars themselves. Moreover, in the limit of small photometric errors, the UV excess selection criterion does not remove any quasars from the BQS sample that are not already removed by the B-band brightness cut (we discuss the impact of the photometric errors below). In other words, the BQS is lacking red quasars not because of its UV excess

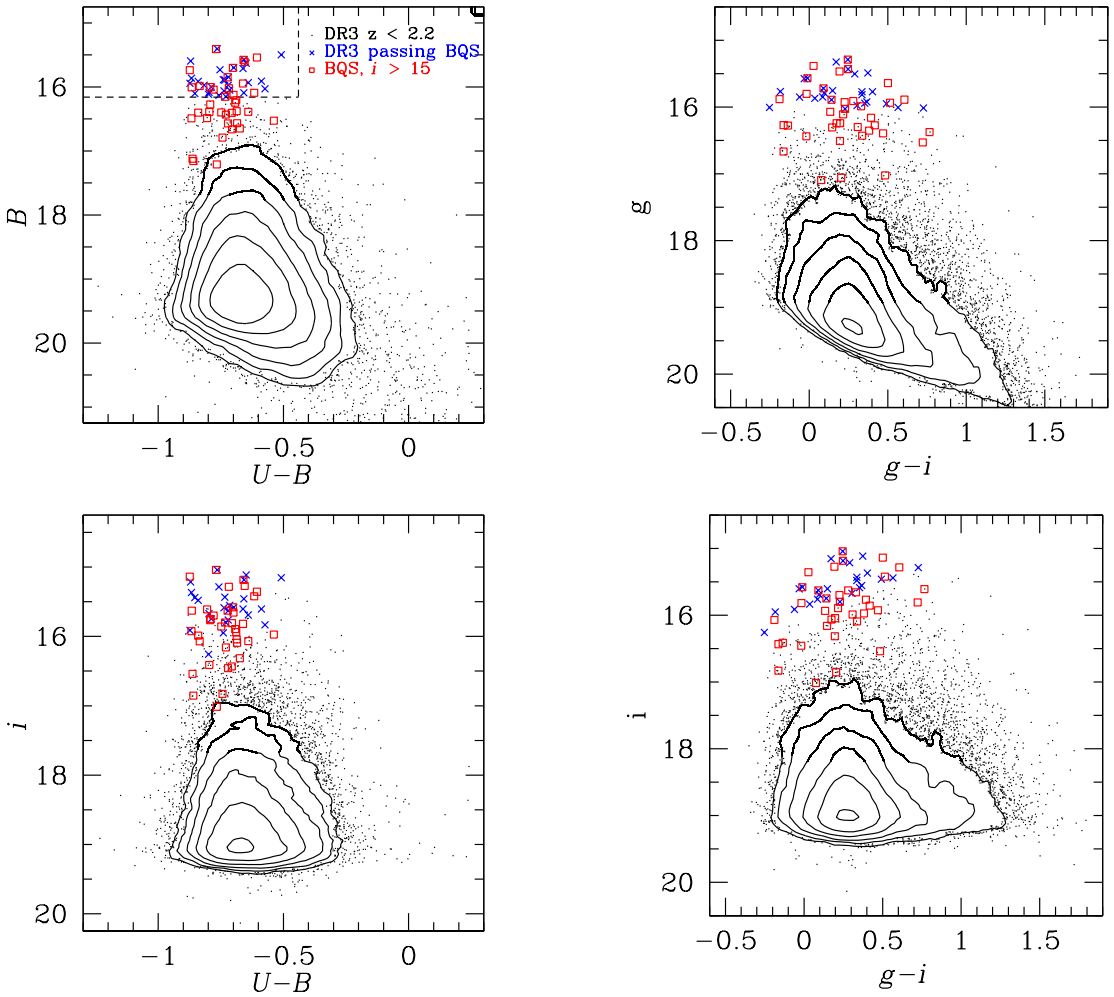

Fig. 10.— Color-magnitude diagrams of SDSS and BQS quasars. *Top left*, B against $U-B$. Top right, g against $g-i$. *Bottom left*, i against $U-B$. *Bottom right*, i against $g-i$ color (we use $g-i$ instead of $g-r$ or $r-i$ because colors derived from neighboring filters have strong features as a function of redshift where an emission line crosses from one filter to the next.). Contours and dots show the DR3 quasar sample, blue crosses are DR3 quasars passing the BQS limits shown by the dashed lines in the top left panel (i.e., $U-B < -0.44$ and $B < 16.16$), and red open squares are SDSS data for the BQS $i > 15$ quasars contained in the SDSS DR3. The correlation between $U-B$ and B at the faint cutoff is a selection effect caused by a combination of the Hα passing through the i filter and host galaxy contamination of quasar colors at low redshifts (see text). The top left diagram shows that the BQS color cut does not remove any objects in addition to the BQS flux limit. The other diagrams show that the more inclusive SDSS quasar candidate selection and the application of a flux limit in i-band include much redder quasars at bright i-band magnitudes than the BQS criteria, in particular compared to the BQS-like quasars selected from the SDSS.

criterion, but because *there are no red quasars which are bright in B*.

This can be understood by considering the shape of the $U-B$ distribution at fixed B. The quasar density peaks at a constant $U-B \approx -0.67$ at all B, and the dropoff in density towards both redder and bluer colors is also independent of B (the contours in the flanks of the distribution are roughly parallel to each other down to $B \approx 20$, where the cutoff becomes skewed as discussed above). Since the number counts of quasars fall rapidly with increasing brightness, nearly all BQS quasars are drawn from near the mode of the UV color distribution. To find significant numbers of both redder *and bluer* quasars than contained in the BQS, it is simply necessary to sample fainter magnitudes (or a larger volume of the Universe — in fact, a much larger volume than is actually available). Thus, the BQS criteria do not produce any color bias when considering only the UV colors of quasars that are bright in B-band. However, the i against $U-B$ and i against $g-i$ CMDs shows that the BQS criteria do introduce a color bias against red quasars which are bright in i-band.

The SDSS selects such red quasars simply because it applies the brightness limit in the i-band. The faintest (in i) BQS-like SDSS quasar has $i = 16.26$. There are only 26 DR3 quasars passing the BQS criteria, but there are 109 DR3 quasars with $i < 16.26$ (even after rejecting extended sources, there are still 64 such quasars). Of the 109 sources, 96 have $U-B < -0.44$, while the remaining 13 redder quasars have colors extending to $U-B = -0.26$ (5 of these are point sources). A Kolmogorov-Smirnov (KS) test comparing the $g-i$ distributions of the BQS quasars and of all SDSS quasars at $i < 16.26$ rejects the hypothesis that they are indistinguishable at $> 99\%$ confidence level; the $U-B$ distributions are formally just indistinguishable (only 86% confidence level for a rejection), but the $U-B$ distribution of the $i < 16.26$ SDSS quasars clearly extends to redder colors than that of the BQS and BQS-like quasars. Thus, the BQS selection criteria lead to the omission of quasars with red colors. This bias is not driven primarily by the UV excess criterion, but instead by application of the magnitude limit in the B-band.

We now return to the comparison of the of BQS-like SDSS quasars and actual BQS quasars. Figure 11 compares the redshift and color distributions of the 39 $i > 15$ BQS objects inside the DR3 area to that of the 26 BQS-like SDSS quasars. The redshift distributions are indistinguishable by the KS test, which returns a very high probability for obtaining both observed distributions as realizations of the same underlying distribution. In fact, the redshift distribution of the BQS quasars is indistinguishable at 95% confidence level from that of DR3 quasars with $U-B < -0.44$ down to $B = 17.0$. The distributions of $U-B$ and $g-i$ are similarly indistinguishable between the BQS and the BQS-like SDSS quasars. Even though the BQS has relatively large color and magnitude errors and a number of quasars are scattered into and out of the sample, the optical properties of BQS quasars are not

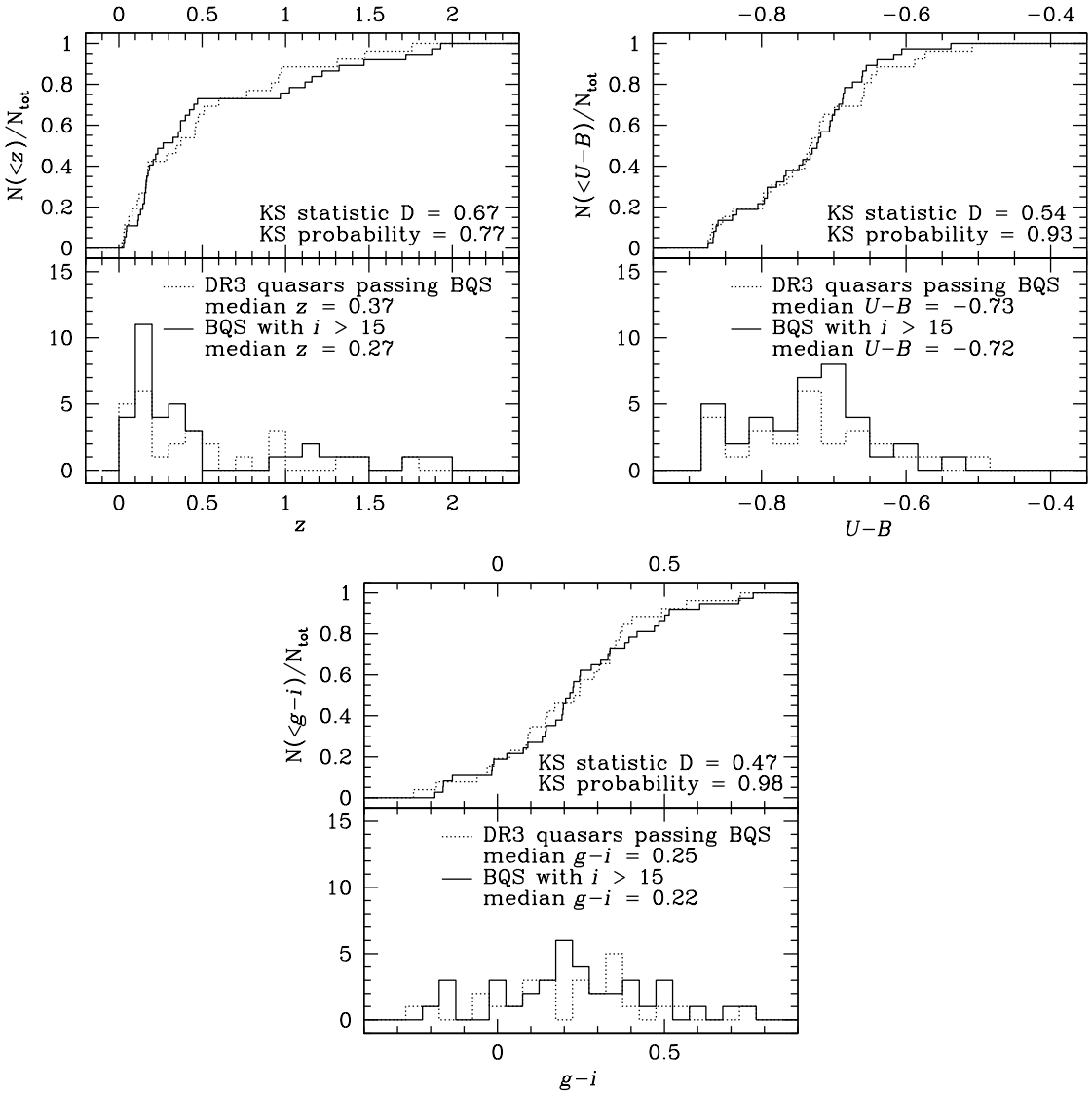

Fig. 11.— Comparison of redshift, $U-B$ and $g-i$ cumulative and differential distribution of $i > 15$ BQS quasars (dotted lines) and DR3 quasars passing BQS criteria (solid lines). All three distributions are indistinguishable.

statistically distinguishable from BQS-like SDSS quasars. Thus, based on our comparison sample, the BQS is a representative survey of bright, blue quasars.

To summarize: Of the SDSS quasars above some limiting i, only the bluest ones are bright enough in B to pass the BQS B-band cut. Therefore, the BQS flux cut excludes most SDSS quasars which have comparable i-band magnitudes as the i-faintest BQS objects. Only an additional 10% are redder than the BQS *color* cut. To recover the red end of the quasar color distribution, it would be necessary to extend the search to fainter B magnitudes *in addition to* relaxing the UV color excess criterion.

4.2. Radio properties

4.2.1. Continuum properties

We next consider the radio properties of the quasars using matches to SDSS data from the FIRST survey. The FIRST survey itself has a flux limit (1 mJy at 1.4 GHz) which introduces selection effects in addition to those from the quasar surveys. Use of the FIRST data is preferable over the use of dedicated radio observations of the BQS because it provides a homogeneous data set for comparing the radio properties of the SDSS quasars to those of the BQS quasars. Since various claims of a radio-loud/radio-quiet bimodality have been made based on the radio flux (Kellermann et al. 1989), radio/optical ratio (e.g., Strittmatter et al. 1980; Ivezić et al. 2002) and the radio power P (e.g., Peacock et al. 1986; Miller et al. 1990, 1993), we begin by considering these three quantities as a function of redshift. We use the integrated FIRST flux of all objects and (following Ivezić et al. 2002) define a FIRST AB magnitude

$$t = -2.5 \log \frac{f_{\rm FIRST}}{3631{\rm Jy}}$$

and the logarithmic radio-optical ratio (without any K-correction)

$$R = 0.4(B - t). \tag{2}$$

The FIRST limiting flux of 1 mJy corresponds to $t = 16.40$.

Figure 12 shows the distributions of radio flux, power, and radio-optical ratio for DR3 and BQS quasars. There are no obvious gaps in any of the distributions which would reveal a strong bimodality in the radio properties of optically selected quasars. Note, however, that the distributions are influenced by the selection limits in *both* the optical and radio surveys. For example, objects with small value of R are concentrated at low redshift because the lowest R is obtained for the objects which are brightest in B, which are concentrated

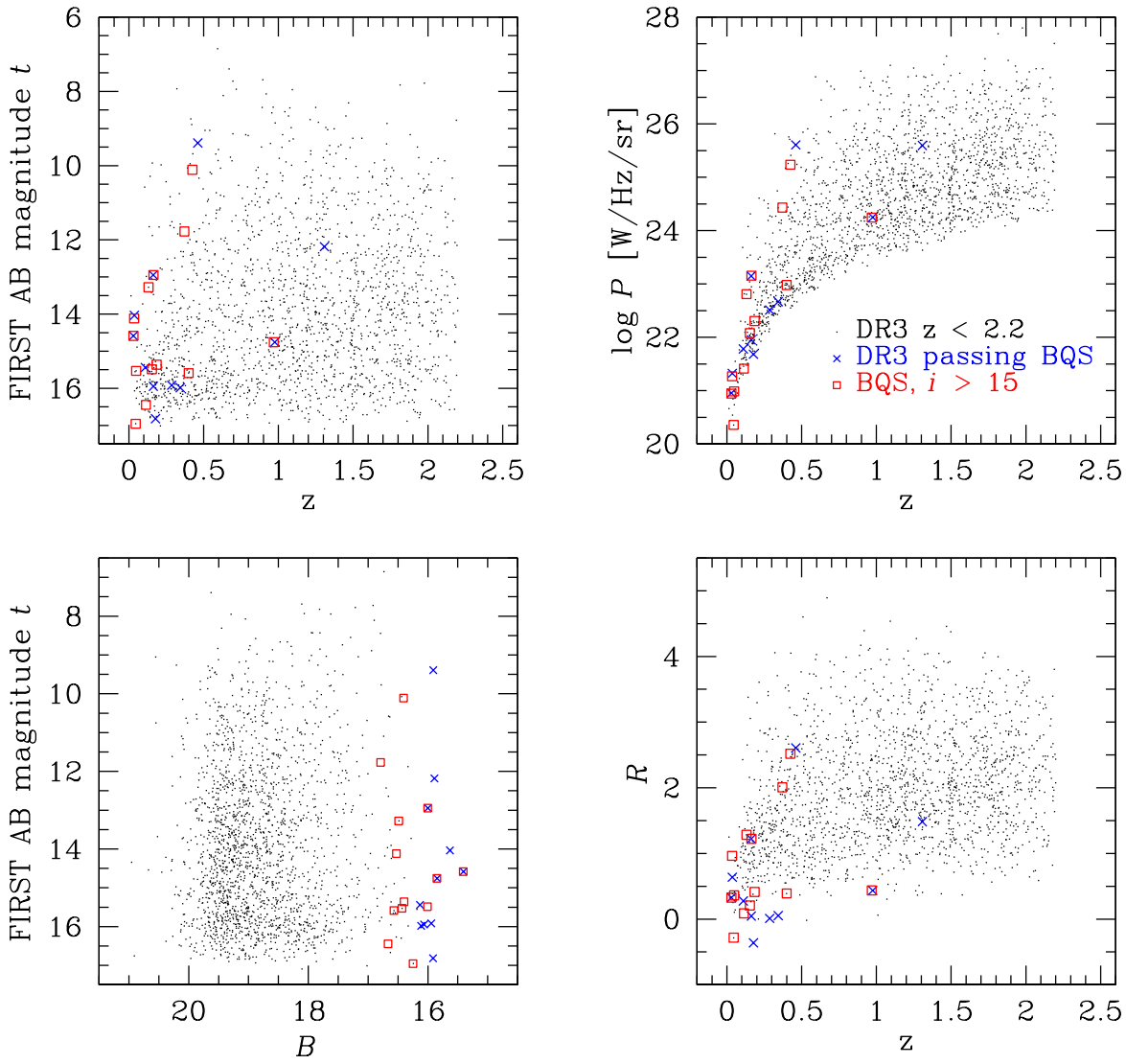

Fig. 12.— FIRST properties of SDSS and BQS quasars, showing integrated radio flux expressed as AB magnitude t (top left), core radio power P (top right), radio-optical ratio $R = 0.4(B - t)$ (without any K-correction, bottom right) against redshift, as well as radio AB magnitude against B magnitude (bottom left). Symbols as in previous figures. There are no obvious gaps in any of the distributions, which are, however, subject to all selection effects of both the SDSS/BQS and the FIRST surveys. The R distribution is most severely affected because objects below the flux limit of either survey can have any value of R. The concentration of low-R points at low z is caused by the increasing number of sources which are bright in B towards low redshift (compare Figure 8).

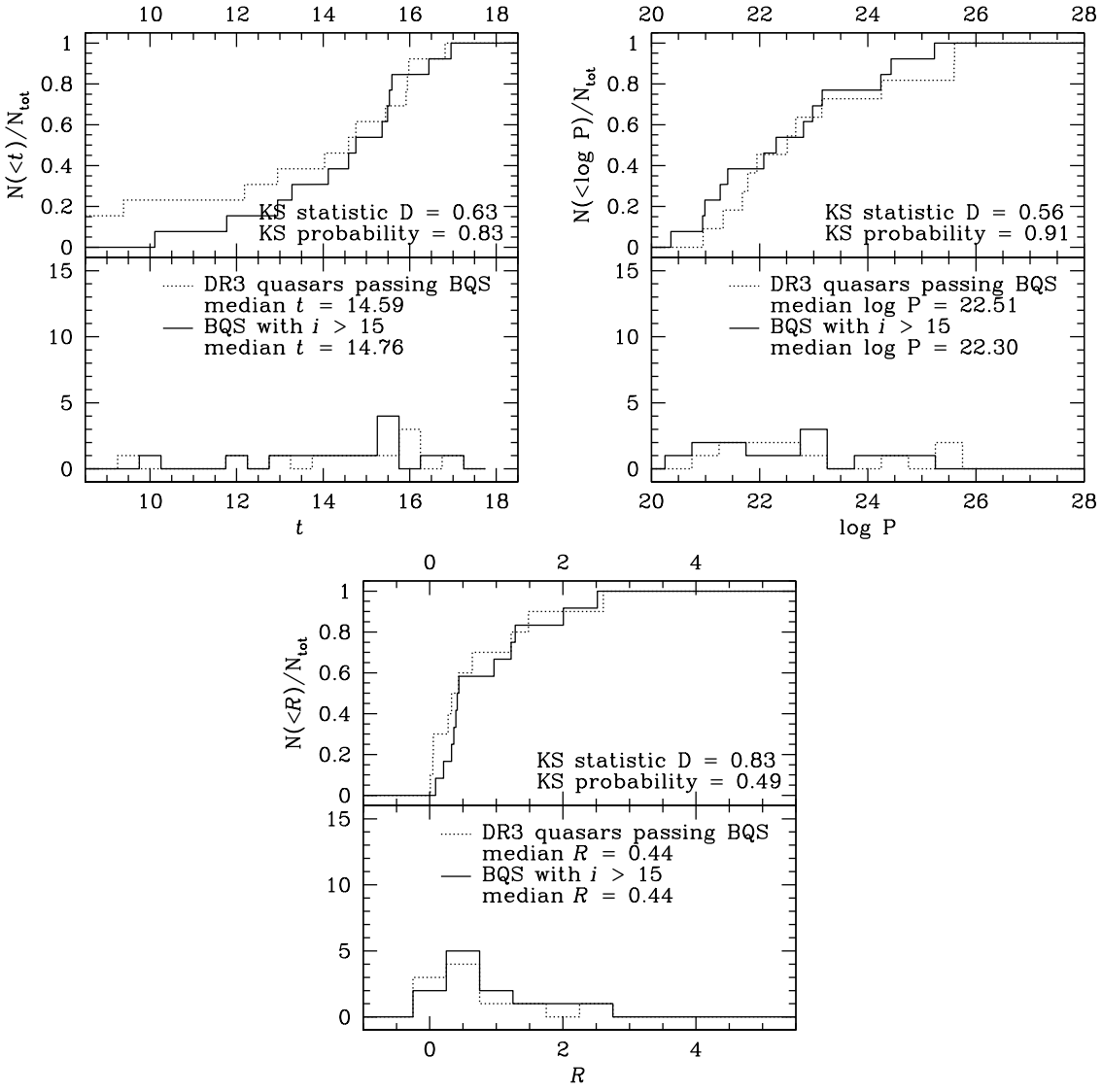

Fig. 13.— Comparison of the radio properties of $i > 15$ BQS objects (dotted lines) and DR3 quasars passing BQS criteria (solid lines). The distributions in FIRST AB magnitude t, radio power P and radio-optical ratio $R = 0.4(t - B)$ are indistinguishable between the two sets of quasars.

at low redshift. Figure 13 compares the distributions of t, $\log P$, and R for the two sets of quasars. In all three cases, the distributions are again statistically indistinguishable, with KS probabilities of 0.83, 0.91, and 0.49 for obtaining the observed t, $\log P$, and R distributions, respectively, from the same underlying distribution. Thus, we find no evidence for any radio dependence of the BQS incompleteness.

We noted above that the $g-i$ distribution of the 26 BQS-like SDSS quasars is different from that of all 109 SDSS quasars with $i < 16.26$, the faintest i magnitude of the BQS-like quasars. However, according to KS-tests, the radio properties of these two samples are entirely indistinguishable. We will return to this point in the next section, where we briefly consider the relation between emission-line properties and radio emission of objects in our BQS-like sample.

4.2.2. Possible BQS biases with respect to radio properties

As noted in the introduction, Miller et al. (1993) stressed "the rarely appreciated fact that, at $z \sim 0.3$, about 50 per cent of the brightest optically selected quasars ... are steep-spectrum, radio-loud objects" (these authors use the [OIII] 5007 narrow-line luminosity to define "brightest", i.e., in fact they appear to mean "most luminous", and use an emission-line quantity rather than a continuum measure such as the continuum flux at a fixed rest-frame wavelength or the B-band magnitude). Their footnote cautioning that this number might be spuriously high if the BQS incompleteness favored the inclusion of radio-loud objects has been interpreted as *suggesting* such a radio-dependent incompleteness — however, these interpretations have not been supported by any additional evidence. In fact, we determined in the previous section that the BQS incompleteness appears to be random with respect to radio properties, given that BQS-like DR3 quasars have indistinguishable distributions of FIRST flux, luminosity, and radio-to-optical flux ratio. However, if the radio and optical properties of all or some quasars are correlated in some way, the BQS sample may not be a random sample of quasars with respect to radio properties.

As a rough check of their finding, we computed $L_{[\mathrm{OIII}]5007}$ from the [OIII]5007 flux determined by the SDSS pipeline and our custom spectral-line fitting routine (Stoughton, Vanden Berk, & Jester, in preparation) for all SDSS quasars with $z < 0.5$ and $B < 17$, where we used a fainter flux limit to increase the sample size to 116 objects. All objects which Miller et al. (1993) classified as "classical double radio sources" (their category D), i.e., radio-loud objects, have $L_{[\mathrm{OIII}]5007} > 5 \times 10^{35}\,\mathrm{W}$.[6] In our sample, there are 13 sources

[6]Miller et al. (1993) used a cosmology with $H_0 = 50\,\mathrm{km/s/Mpc}$, $\Omega_m = 0$, and $\Omega_\Lambda = 0$, resulting in

with $L_{[OIII]5007} > 5 \times 10^{35}$ W. Of these, four have a detection of FIRST flux at the optical position. Inspection of FIRST and NVSS (Condon et al. 1998) images and a literature search reveal that three are "classical double" radio sources (4C +31.30, 4C +60.24 = 3C 351, and 4C +61.20); the fourth radio source has compact radio emission associated with the core, but no clear lobes. The remainder of the [OIII]-luminous sources have no radio emission detected in FIRST, NVSS, or the literature, but all have upper limits on the FIRST luminosity lying below the luminosity of the three double-lobed sources. The Miller et al. (1993) prediction was that 6.5 of the sources (50% of 13) should be double radio sources, but we found only 3. The Poisson probability to obtain 3 events where 6.5 are expected is 6.9%. Thus, our investigation of BQS-like objects does not allow us to rule out the Miller et al. (1993) result.

In order to obtain some clue as to what causes the large fraction of radio-loud objects at the high-[OIII] luminosity end of the BQS and our BQS-like sample, we have constructed a comparison sample of SDSS quasars using a bright i-band cut $i < 16.34$, which contains a similar number of objects as the $B < 17$ sample just employed. This i-band cut removes about 50% of the sources with $L_{[OIII]5007} > 10^{35}$ W that were present in the B-band limited sample, including one of the three double-lobed sources mentioned above (4C +61.20). Of those objects in the B-band limited sample, the bluest (in $B - i$) are missing in the i-band limited one. Thus, there is some indication that quasars with a bluer continuum are more likely to be luminous in [OIII] 5007. If the link between radio and narrow-line luminosity identified by Miller et al. (1993, also see Willott et al. 1999) indeed holds for all quasars, the BQS is biased towards the inclusion of radio-loud objects because it preferentially includes objects which are luminous in [OIII] 5007. This would be consistent with the trend for more luminous quasars to have bluer optical/UV continua (Carballo et al. 1999, e.g.). However, an apparently contradicting observation is that the radio-loud objects among the SDSS color-selected quasar sample (defined as having $R > 1$, where R is given by Equation 2) have *redder* $g - i$ colors than those with $R < 1$ (see Richards et al. 2001). A more detailed investigation of these connections between [OIII] luminosity, radio morphology and continuum properties will require the analysis of a larger sample of bright quasars from the SDSS, and ideally complete radio imaging of an SDSS-defined bright quasar sample.

4.3. Summary of SDSS-PG comparison

In summary, we find the following answers to the two questions posed at the beginning of §4:

---

luminosities about a factor 2 greater than those in the current standard cosmology.

1. The distributions in redshift, $U-B$, $g-i$, radio magnitude t, core radio power P, and radio-optical ratio R of the 39 BQS quasars with $i < 15$ inside the SDSS DR3 area are indistinguishable from those of the 26 SDSS DR3 quasars passing the BQS criteria. Thus, we find no evidence that the incompleteness of the BQS is biased with respect to radio or optical properties. We compare this finding to previous investigations of the BQS incompleteness in §5.1 below.

2. The BQS selection effects are predominantly caused by application of a flux limit in the B-band. All DR3 quasars passing the BQS flux limit also pass the color cut $U-B < -0.44$. However, the BQS limits introduce a bias against red objects relative to the SDSS sample when considering the colors (both $U-B$ and $g-i$) as a function of i-band magnitude (or equivalently, the BQS would sample the red part of the quasar population only if it was extended to fainter magnitudes). Thus, the application of optical flux limits at different wavelengths introduces a bias that is comparable to radio flux limits applied at different wavelengths: flat-spectrum (blue) sources are preferentially included in high-frequency (B-band) selected surveys, while the sample misses significant numbers of objects with comparable low-frequency (i-band) luminosities and steeper (redder) spectra. We discuss in §5.2 below whether this bias is remedied by moving the flux-limiting bandpass to ever longer wavelengths.

Thus, the BQS is representative for quasars which are bright in the B-band, but it is clearly *not* representative even of quasars which are bright in i-band.

5. Discussion

5.1. Comparison to other determinations of BQS completeness

5.1.1. Color and magnitude incompleteness

Wampler & Ponz (1985) presented one of the first investigations of the BQS completeness. Their main concerns were a possible color incompleteness biasing against the inclusion of redder objects, and that some of the PG limiting magnitudes might actually have been much fainter than stated by Schmidt & Green (1983). Similarly, Wisotzki et al. (2000) noted a possible faint-end overcompleteness of the BQS relative to the stated flux limits. Our comparison of SDSS and PG photometry in §2 and our investigation of the PG completeness relative to an SDSS-selected sample of UV excess sources in §3 confirm both of these suggestions: the recalibration of PG photographic magnitudes we found necessary (Figure 3) agrees with that suggested by Wampler & Ponz (1985) and Wisotzki et al. (2000), with the

PG overestimating the flux of faint objects. However, we can rule out a *constant* offset in the B magnitude such as the one reported by Goldschmidt et al. (1992). We also found that the PG limiting $U-B$ color is in fact closer to $(U-B)_{\rm lim} = -0.71$ than to the intended $(U-B)_{\rm lim} = -0.44$ (Figure 7). This leads to an increased bias against quasars in the redshift range $0.5 < z < 1$, where their median $U-B$ colors make an excursion into the red (Figure 9) due to the presence of the MgII emission line in the B filter (compare Wampler & Ponz 1985).

Since the $U-B$ distribution of bright quasars peaks at $U-B \approx -0.7$ (Figure 10), applying the (revised) BQS color cut $(U-B)_{\rm lim} < -0.71$ removes about 50% of the quasars that should be in the sample. As long as the color distribution is roughly symmetric about the mode, this statement is true whatever the photometric error may be; since the 2-σ PG photometric error actually encompasses the entire width of the $U-B$ distribution at bright B, the detection probability in the BQS will be approximately independent of $U-B$. Hence, the incompleteness of the BQS will be mostly random with respect to $U-B$ color, except for a bias against quasars with $0.5 \lesssim z \lesssim 1.0$, where the median $U-B$ color reaches -0.5.

In this context, it is important to recall that the majority of bright quasars are found at $z < 0.5$ in any case. This is true for the BQS, the HEQS (Wisotzki et al. 2000) and the SDSS quasar survey. Thus, while the color-redshift relation of quasars certainly introduces a bias against intermediate-redshift objects in the BQS, these objects are inherently rare in the BQS and fainter surveys are necessary for an accurate determination of the quasar space density at $z > 0.5$.

5.1.2. What is the surface density of bright quasars?

Short of a determination of the surface density of bright quasars from the SDSS which requires a detailed analysis of the SDSS completeness to quasars (Vanden Berk et al. 2005; Richards et al. 2005, in prep.), our best estimate of the surface density incompleteness of the BQS is roughly 50% because the corrected $U-B$ cut of -0.71 approximately bisects the $U-B$ distribution of bright quasars (Figure 10). Wisotzki et al. (2000) have presented the most comprehensive discussion to date of the BQS incompleteness in terms of surface density. They find 1.48 times as many quasars per square degree, i.e., an incompleteness of 32%, but cautioned that the true incompleteness may be as large as 50% if SG83 underestimated the Eddington bias; this is indeed the case if our B recalibration is correct, since it makes the faint plate limits even fainter. A similar number (53%±10%) was obtained by Mickaelian et al. (2001) in their most recent analysis of the First Byurakan Survey, although these authors caution that their survey area was rather small and results should not be taken as

definite. Kilkenny et al. (1997) find a similar surface density of UV excess objects in the Edinburgh-Cape survey as in the PG. Thus, the report by Goldschmidt et al. (1992) of a surface density of quasars exceeding that of the BQS by a factor of three seems to be an outlier. We could only speculate on possible explanations, but small-number statistics in combination with the revised $U-B$ cut and the large photometric errors in the PG may be sufficient to explain the large discrepancy. We also note that the formal significance of the surface density difference between EQS and BQS shown in Figure 1 of Goldschmidt et al. (1992) is less than 2σ.

In this context, let us reconsider what is meant by the term "effective magnitude limit". Figure 1 shows that the value $B_{\rm eff} = 16.16$ is close to the area-weighted median limiting magnitude. However, this is not the same as the magnitude to which a uniform quasar survey yields the same number of objects as the entire BQS, with its magnitude limit that is varying from plate to plate. If number counts of quasars increase with limiting apparent magnitude m as $10^{\beta m}$, the effective limiting magnitude of a survey with a set of limiting magnitudes m_i and total area surveyed to that limiting magnitude A_i is

$$\frac{1}{\beta}\log\left(\frac{\sum_i A_i 10^{\beta m_i}}{\sum_i A_i}\right)$$

Using any value for β from 0.77 (Wisotzki et al. 2000) to 0.9 (Schmidt & Green 1983) with the areas and limiting magnitudes of the PG fields from Green et al. (1986) results in an effective limiting magnitude of $B_{\rm eff} = 16.20$ (rounded to two decimal places), which would imply an increase in the expected surface density of the BQS of 7.4%–8.6%, and hence a corresponding decrease in all completeness estimates.

In summary, most recent determinations of the surface density of B-bright quasars point to a surface density completeness of the BQS of 50% or more. This agrees with our expectation of an incompleteness of roughly 50% introduced by the revised BQS color cut $(U-B)_{\rm lim} = -0.71$, which bisects the color distribution of bright quasars. We found no strong differences between optical and radio properties of BQS and BQS-like SDSS quasars. Thus, we find no evidence for any systematic effects other than those caused by the color and magnitude cuts and errors.

5.2. Is there an optimal wavelength for applying quasar flux limits?

Quasar surveys need efficient photometric candidate selection criteria to avoid the high cost associated with taking spectra of many false positives included in the candidate list. By construction, our view of the quasar population (and more generally, the population of

active galactic nuclei, AGN) is restricted to those objects whose SED satisfies the selection criteria. The most fundamental such restriction is the application of a flux limit at a certain wavelength. We have already alluded to the fact that the SDSS detects redder quasars with comparable i-band magnitudes as BQS objects solely by virtue of applying the flux limit in the i-band (§4), in the same way as high-frequency (4.85 GHz, 6 cm) radio surveys miss steep-spectrum radio sources that are picked up at low frequencies (178 MHz, 1.7 m). If in addition there are correlations between the properties of quasars in different parts of the electromagnetic spectrum, optical survey selection criteria may lead to biases in our understanding of the radio or X-ray properties of quasars (see §4.2.2). In this section, we address the question whether there is an optimal waveband for applying flux limits in quasar surveys that would reveal the "true" quasar population.

The above results confirm the expectation that the application of a B-band flux limit biases the BQS against the inclusion of quasars with redder continua, which the i-band limited SDSS survey detects. Here, we first consider whether the SDSS could be missing any large population of highly reddened Type 1 AGN, and then address the question whether quasar selection could be further improved relative to the SDSS selection algorithm by moving the flux-limiting band to even longer wavelengths.

The basic problem in optical selection of quasar candidates is that the success of the unified scheme for active galactic nuclei (Antonucci 1993; Urry & Padovani 1995; Haas et al. 2004a) implies that orientation-dependent obscuration shapes our optical and soft X-ray view of AGN, so that only the hard X-ray and mid-infrared wavelength regions yield an isotropic measure of an AGN's luminosity. High-sensitivity space observatories such as Spitzer, XMM and Chandra which probe these wavelength regions certainly allow the reliable identification of heavily extincted quasars with high dust masses (see Haas et al. 2004b; Lacy et al. 2004, e.g., for promising mid-infrared selection strategies). However, large-area surveys are only possible at optical and near-infrared wavelengths, even though such quasar surveys can only detect the low-obscuration part of the quasar population as a matter of principle. However, there is a class of mildly obscured ("reddened") quasars, in which internal dust extinction both diminishes the observed flux and reddens the observed color, which may still be accessible to optical selection.

The SDSS selection criteria (Richards et al. 2002) mitigate both problems, the reddening problem by targeting *all* objects with non-stellar colors as quasar candidates, and the extinction problem by using i-band selection, in which the extinction always has a smaller impact than in the B-band. Richards et al. (2003) showed that the SDSS color selection is still sensitive to quasars with E_{B-V} as large as 0.5, although objects will still be lost if they are extincted to below the survey flux limit. Similarly, Hall et al. (2002) identified

several highly reddened broad absorption-line quasars in the SDSS quasar sample, nearly all of which were targeted as quasar candidates. It is instructive in this context to see how SDSS target selection treated the *Deeprange* I-band selected FIRST-detected quasars from White et al. (2003). Thirty-two of these quasars are inside the SDSS DR3 area. All but six are identified as quasar candidates by SDSS color selection; of these six, two are still targeted as FIRST sources. The other four untargeted objects, as well as all but four of the color-selected candidates, are too faint to be included in the spectroscopic survey. Thus, while there certainly are low-luminosity quasars that are not included in the SDSS survey because of its flux limit, we see no reason to support "the hypothesis that radio quasars are dominated by a previously undetected population of red, heavily obscured objects" (White et al. 2003) — this population has remained undetected in SDSS not because of their red color, but (along with other, less luminous quasars) because of their faintness.

Glikman et al. (2004) found 17 highly reddened quasars ($B - K > 6.5$) over an area of 2716 deg^2 by searching for FIRST radio sources without optical counterpart in the first-generation Palomar Observatory Sky Survey; similar to the *Deeprange*-selected quasars, these are mostly too faint for inclusion in the SDSS quasar survey. Nine of them are inside the DR3 coverage, three of the fainter ones are recognized as quasar candidates, but below the spectroscopic brightness limit; however, the brighter ones (three objects) were rejected as quasar candidates because they have the colors of white-dwarf + M-star binaries. Still, Richards et al. (2003) have shown that these moderately reddened quasars only add about another 10% to the number counts at their unextincted magnitude. These authors have also shown that the hidden population of heavily obscured X-ray emitting AGN which is necessary to account for the hard X-ray background (see Treister et al. 2004, e.g.) is not simply a smooth extension of the mildly reddened population towards greater optical depths, again because the distribution of continuum colors in the SDSS allows only a small fraction of dust-reddened objects (see also Hopkins et al. 2004). Instead, the heavily obscured objects are more likely to appear as Type 2 AGN without a strong quasar continuum or broad emission lines, to which optical quasar surveys are typically insensitive (although they *can* be identified in SDSS spectra by a dedicated search; see Zakamska et al. 2003).

Thus, having moved beyond traditional UV excess color selection such as that employed by the BQS, the SDSS quasar survey *is* sensitive both to red quasars (those with steep continua) and reddened quasars (those with spectral curvature induced by internal dust reddening). Still, the possibility remains that selection in an even longer-wavelength band, for example the near-infrared K-band at 2.2 μm, will uncover objects with similar K-band magnitudes as some of the SDSS quasars, but even steeper continuum slopes that cause them to remain undetected at the SDSS's i-band flux limit. This suggestion has been made by Francis et al. (2000), who use the optical colors of a radio-selected sample to show

that extinction is likely to give the reddened quasars a color close to the stellar locus, but that the addition of a near-infrared filter can break the degeneracy between stellar and quasar colors (although again, only 10% of their sample are reddened quasars or radio galaxies). Similarly, Warren et al. (2000) suggest a "K-band excess" (KX) method to select quasar candidates, exploiting the fact that a quasar's SED continues to rise towards longer wavelengths, while the single-temperature black-body SED of stars turns over shortward of the K-band (however, the K-band flux of lower-luminosity quasars will again suffer from contamination by host-galaxy starlight). Fortunately, the cross-matching of the SDSS quasar catalog with data from the 2MASS survey allows us to extend the wavelength coverage of the SDSS into the near-infrared. The following analysis of the 2MASS K-band magnitudes for optically selected quasars from the SDSS DR3 quasar catalog (Schneider et al. 2005) shows that it is extremely unlikely that a significant population of such objects exists (also see Francis et al. 2004).

Quasar SEDs have a local minimum at $\sim 1\,\mu$m which separates non-thermal emission with a power-law spectrum at shorter wavelengths from thermal dust emission at longer wavelengths (see Koratkar & Blaes 1999, e.g.). The K-band samples the dust emission at redshifts up to $z \approx 1.2$ and the non-thermal power-law emission at higher redshifts, so a division of the quasar sample at $z = 1.2$ approximately divides the sample by K-band emission mechanism. Furthermore, to avoid contamination of the optical and in particular the K-band flux from starlight, we restrict the analysis to objects at redshift $z > 0.6$. There are 26777 color-selected quasars at redshift $z > 0.6$ in the DR3 catalog. Of these, only 3047 are detected in the 2MASS point-source catalog, with K magnitudes extending down to 17.35 (*all* SDSS quasars brighter than $i = 16.15$ are detected by 2MASS). Any putative extremely red quasars will be close to the i-band cutoff of the SDSS but well above the K-band limit of 2MASS.

Figure 14 shows the SDSS i against 2MASS K for the brightest 10% of the objects in the K-band in either redshift interval. In both redshift intervals, there are only few objects that are bright in K but not also bright in i. The i and K magnitudes are remarkably correlated, typically $i - K \approx 2.7$. Only a small fraction of objects have $i - K > 3.5$ in the SDSS-2MASS matched sample, even though the SDSS i-band limit would have allowed the detection of such objects at the brightest K-band magnitudes. Inspection of their spectra shows more red continua than among typical SDSS quasars, and many have redshifts close to the lower limit of $z = 0.6$, suggesting that there is some host galaxy contamination. Even if a quasar's colors became indistinguishable from those of stars, causing it to fail the color selection criteria, the targeting of FIRST point-source counterparts would have recovered at least the radio sources among the heavily reddened objects.

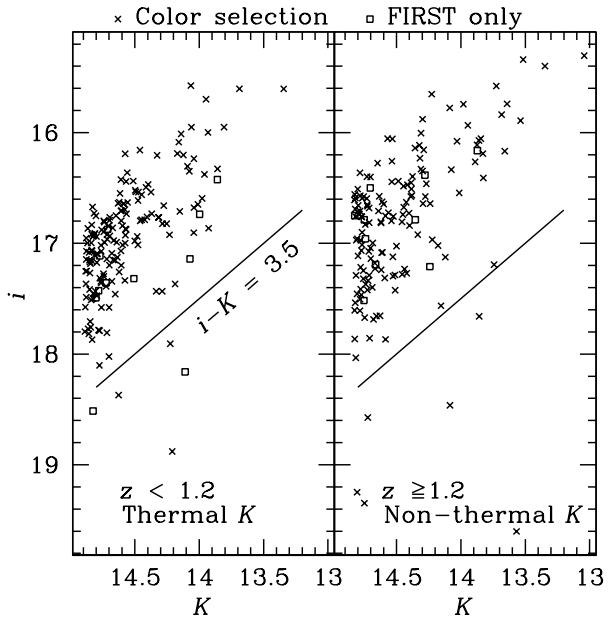

Fig. 14.— SDSS i-band magnitude of SDSS DR3 quasars plotted against 2MASS K-band magnitude, both corrected for galactic extinction. Only objects at $z > 0.6$ are shown to avoid contamination by starlight. Each panel shows the brightest 10% of objects in the K-band (140 in the left-hand panel, 180 in the right-hand panel). Crosses show color-selected objects, while open squares show objects which fail the color selection but are targeted as point-source counterparts to FIRST sources. At redshifts up to $z \approx 1.2$, the K-band samples thermal emission longward of the 1 μm minimum in quasar SEDs, while it samples the same power-law emission as the i-band at redshifts greater than 1.2. Whatever the K-band emission mechanism, most objects have $i - K < 3.5$, even though the $i > 19.1$ flux limit ($i > 20.2$ for certain regions of optical color space) would have allowed the detection of objects as red as $i - K = 5.5$ at $K = 13.5$, in particular among the FIRST only-selected objects.

Thus, the bright B-band limit in the BQS biases that survey against inclusion of objects from the red end of the distribution of quasar continuum slopes. By contrast, the SDSS i-band flux limit samples the full distribution of quasar continuum slopes, including a small fraction of objects with moderate extinction.

5.3. Science impact of BQS selection effects

Having shown that bright B-band selected quasar surveys (and the PG survey in particular) are biased to the blue and fail to explore the reddest part of the quasar population that appears in surveys with fainter limits, it is important to take stock of the scientific impact of our reliance on such samples. This is important because follow-up studies that require high S/N data, long exposures, and/or good time sampling must necessarily concentrate on the brightest quasars.

The most obvious impact is on that of our understanding of the mean quasar spectral energy distribution (e.g. Sanders et al. 1989; Elvis et al. 1994). The PG sample has a marked influence on these mean SEDs. Further exploration of how fainter, redder quasars fit into the mean SED picture is particularly important given that it is a nearly universal habit to assume that all quasars have exactly the mean SED (even though Elvis et al. (1994) clearly stress that there is a range of SEDs).

The computation of accretion rates ($\propto L_{\rm Bol}/M_{\rm BH}$) generally assumes the mean SED in determining the bolometric correction rather than an SED tailored for each object. Similarly it is important that we reconsider the impact of the PG sample on the determination of black hole masses. The two largest samples of objects on which reverberation analysis has been applied (Wandel et al. 1999; Kaspi et al. 2000) are (necessarily) dominated by bright objects and the Kaspi et al. (2000) sample exclusively consists of PG quasars. The issue here is whether the observed BELR size-luminosity relationship ($R \propto L^{\sim 0.5}$) holds for redder quasars. If the optical/UV colors of quasars are an indication of the temperature of the accretion disk, it may not be unreasonable to expect some scatter in this relationship as a function of color.

The PG sample also impacts our understanding of the X-ray properties of quasars. For example, the Elvis et al. (1994) sample (19/47 PG quasars) was specifically chosen to have good S/N in both their *Einstein* and *IUE* spectra and thus are unlikely to be representative of the typical optical to X-ray ratio, α_{ox}. Furthermore, follow-up studies of quasars in the X-ray are heavily dominated by the sample of low-z PG quasars defined by Laor et al. (1997). In particular it has been recently suggested that *XMM-Newton* spectra of PG quasars reveals

a near universality of the so-called "soft X-ray excess" below 2 keV (Porquet et al. 2004; Piconcelli et al. 2005). Again it is important to test if this feature is indeed universal or only characteristic of bright, blue quasars.

Finally, we emphasize the obvious influence of the PG sample on the so-called "eigenvector" analysis of quasars initiated by Boroson & Green (1992). This study is based on the analysis of the spectral properties of the 87 PG quasars with $z < 0.5$. Boroson & Green (1992) demonstrate that a principal component analysis can be used to define two key eigenvectors that account for the majority of the variance in their sample. While it has been difficult to identify the underlying physical drivers behind these eigenvectors, one suggestion is that they might be accretion rate and black hole mass (Boroson 2002). If red quasars lie *along* the principal component axes as they are currently defined, then existing eigenvector analysis is robust to their addition. If, however, red quasars lie preferentially off-axis, then their inclusion may cause a rotation of the axes that will have implications for the association of the dominant eigenvectors with underlying physical properties.

6. Summary

1. We have presented separate transformations for stars and quasars between the SDSS survey system and Landolt photometry on the Johnson-Kron-Cousins system (§2).

2. A comparison of SDSS photometry and photographic plate-based magnitudes from the Palomar-Green (PG) survey (GSL86) of hot stars (which are not expected to be variable) reveals that the PG magnitudes require recalibration. PG photographic magnitudes are precise in the range $14 \lesssim B \lesssim 16$, but too faint by up to 0.2 at $B \lesssim 14$ and $B \gtrsim 16$. PG photoelectric magnitudes of these objects agree with SDSS magnitudes to within the photometric errors (§2.3.1).

3. The photographic-plate derived $U-B$ colors of the quasars from the PG survey (the objects included in the Palomar-Green Bright Quasar Survey, BQS; SG83) are offset by about 0.2 magnitudes towards the red when compared to SDSS-derived $U-B$ colors. This difference is difficult to explain by variability, thus it is an indication the need to recalibrate the PG $U-B$ colors in addition to the B magnitudes. The average and RMS difference in B-band magnitude between the recalibrated PG and SDSS measurements is consistent with the variability expected over a 30-year epoch difference (§2.3.2).

4. We have simulated the color selection of objects in the PG survey from their parent sample as observed by the SDSS DR3 by computing each object's detection probability from the appropriate PG limiting magnitude, color, and corresponding errors (§3).

The parent sample was defined as all objects which are bluer than the main sequence ($U-B < -0.3$) and covers roughly 3,300 square degrees out of the PG's total survey area of 10,668 square degrees. The distributions of B magnitude, $U-B$ color, and detection probability of the simulated and actual PG survey can only be made to agree if we adjust the limiting color to $(U-B)_{\rm lim} = -0.71$ (in addition to recalibrating the limiting magnitudes as above), and the photographic color error to $\sigma_{U-B} = 0.24$ (smaller than the value given by GSL86, but as given by SG83). The offset between our revised color cut and the cut $(U-B)_{\rm lim} = -0.44$ intended for quasars is similar to the offset in the $U-B$ color determined above. With the original color cut and error, we predict (*post facto*) that 17,000 main-sequence objects are scattered into the PG's photometrically defined sample by photometric errors in color and magnitude. With our revised limits, the number is reduced to 500 objects, which compares well with the actual number of 1125 objects rejected over the full PG area.

5. Comparing the properties of 39 BQS quasars inside the SDSS DR3 area to BQS-like quasars with $B < 16.16$ and $U-B < -0.44$ selected from the SDSS quasar survey (26 objects), we find no statistically significant differences in the distributions in redshift, $U-B$, $g-i$, radio magnitude t, core radio power P, or radio-optical ratio R (§4). Moreover, as the $U-B$ distribution of B-bright SDSS quasars peaks at $U-B \approx -0.7$ and the 2-σ $U-B$ color error is about as large as the width of the color distribution, inclusion or exclusion in the BQS will be essentially random with respect to $U-B$ color, except for a bias against objects in the redshift interval $0.5 \lesssim z \lesssim 1.0$, where the median quasar $U-B$ is much redder than at other redshifts as the MgII line passes through the B-band. However, any bright quasar survey is limited to low-redshift objects, so that few objects from that redshift interval would be included even in the absence of color biases. Thus, we cannot identify any serious systematics to the BQS incompleteness.

6. No SDSS quasar brighter than $B = 16.16$ is *redder* than $U-B = -0.44$, so that the application of the UV excess criterion *with the high photometric accuracy of CCD photometry* does not remove any objects from the sample that have not already been excluded by the application of the B-band flux limit. However, the SDSS quasar survey does include objects which are redder in $U-B$ than the BQS quasars, but have i-band magnitudes similar to those of the BQS objects. Thus, while the BQS incompleteness with respect to its own selection criteria appears largely random, use of the BQS criteria does lead to selection effects compared to a sample defined by an i-band flux limit, such as the SDSS. These selection effects are predominantly caused by application of a flux limit in the B-band and not by the application of a UV color excess criterion. The $U-B$ color distribution of stars is much broader than that of quasars, so that the

PG survey *is* progressively more biased against inclusion of redder stars.

7. Our recalibration of PG B-band magnitudes and colors rules out a constant magnitude offset in the BQS magnitudes as reported by Goldschmidt et al. (1992), but agrees with the color and magnitude biases perceived by Wampler & Ponz (1985) and Wisotzki et al. (2000) (§5.1).

8. Determination of the surface density of bright quasars from SDSS number counts requires detailed analysis of the SDSS quasar selection function which is beyond the scope of this paper. Given the coincidence of the revised color cut $(U-B)_{\rm lim} = -0.71$ with the mode of the quasar $U-B$ distribution down to at least $B = 19$, our best estimate of the BQS surface density incompleteness is roughly 50%.

9. Miller et al. (1993) reported that 50% of the BQS objects at $z < 0.5$ with similarly high $L_{[\rm OIII]5007}$ are steep-spectrum radio-loud objects. Of the SDSS quasars at $z < 0.5$ and $B < 17$, thirteen have an [OIII] 5007 narrow-line luminosity of above 5×10^{36} W; three of these are "classical double" radio sources (§4.2.2). The Poisson probability for obtaining 3 sources where 6.5 are expected is 6.9%. It is necessary to investigate the radio and emission-line properties of a larger sample of SDSS-selected quasars in order to obtain a more significant rejection or confirmation of the Miller et al. (1993) result.

10. Considering the brightest 10% of the SDSS objects in the 2MASS K-band, we find that very few optically selected quasars are bright in K, but faint in i (§5.2); most SDSS quasars have $i - K \approx 2.7$. Thus, there can only be a numerically small population of reddened objects which are still recognizable as Type 1 quasars. This finding is in line with previous analyses of the color distribution of SDSS quasars (Richards et al. 2001; Hopkins et al. 2004). The use of an i-band flux limit allows us to sample a much larger range of continuum colors of optically selectable quasars than the BQS B-band limit. The i-band magnitude appears as fundamental a measure of a quasar's total energy output as its K-band magnitude, whether the K-band flux samples the same power-law emission as the i-band (at $z \lesssim 1.2$) or thermal dust emission ($z \gtrsim 1.2$).

11. Results that have been obtained for PG quasars are commonly assumed to be representative for the entire quasar population in fundamental issues such as SED shapes, the determination of black hole masses via reverberation mapping and related scaling relations, quasar X-ray properties, and the physical drivers behind the Boroson & Green (1992) eigenvectors. Given that our work here shows that the BQS quasars are just the bright, blue tip of the quasar iceberg, it appears prudent to reassess the impact of the BQS sample selection on these results, and to cross-check them for a wider range of spectral shapes than encountered among the BQS quasars.

SJ and CS were supported by the US Department of Energy under contract No. DE-AC02-76CH03000. DPS and DEVB were partially supported by National Science Foundation grant AST03-07582, and MAS was supported by grant AST03-07409. SJ is grateful for the hospitality of the Princeton University Observatory, where this paper was completed. This research has made use of: NASA's Astrophysics Data System; STSDAS/synphot and PyRAF, products of the Space Telescope Science Institute, which is operated by AURA for NASA; data products from the Two Micron All Sky Survey, which is a joint project of the University of Massachusetts and the Infrared Processing and Analysis Center/California Institute of Technology, funded by the National Aeronautics and Space Administration and the National Science Foundation.

Funding for the creation and distribution of the SDSS Archive has been provided by the Alfred P. Sloan Foundation, the Participating Institutions, the National Aeronautics and Space Administration, the National Science Foundation, the U.S. Department of Energy, the Japanese Monbukagakusho, and the Max Planck Society. The SDSS Web site is http://www.sdss.org/. The SDSS is managed by the Astrophysical Research Consortium (ARC) for the Participating Institutions. The Participating Institutions are The University of Chicago, Fermilab, the Institute for Advanced Study, the Japan Participation Group, The Johns Hopkins University, the Korean Scientist Group, Los Alamos National Laboratory, the Max-Planck-Institute for Astronomy (MPIA), the Max-Planck-Institute for Astrophysics (MPA), New Mexico State University, University of Pittsburgh, University of Portsmouth, Princeton University, the United States Naval Observatory, and the University of Washington.

REFERENCES

Abazajian, K., et al. 2004a, AJ, 128, 502

Abazajian, K., et al. 2003, AJ, 126, 2081

—. 2004b, AJ, accepted [astro-ph/0410239]

Antonucci, R. 1993, ARA&A, 31, 473

Becker, R. H., White, R. L., & Helfand, D. J. 1995, ApJ, 450, 559

Blanton, M. R., Lin, H., Lupton, R. H., Maley, F. M., Young, N., Zehavi, I., & Loveday, J. 2003, AJ, 125, 2276

Boroson, T. A. 2002, ApJ, 565, 78

Boroson, T. A., & Green, R. F. 1992, ApJS, 80, 109

Carballo, R., González-Serrano, J. I., Benn, C. R., Sánchez, S. F., & Vigotti, M. 1999, MNRAS, 306, 137

Condon, J. J., Cotton, W. D., Greisen, E. W., Yin, Q. F., Perley, R. A., Taylor, G. B., & Broderick, J. J. 1998, AJ, 115, 1693

Croom, S. M., Smith, R. J., Boyle, B. J., Shanks, T., Miller, L., Outram, P. J., & Loaring, N. S. 2004, MNRAS, 349, 1397

de Vries, W. H., Becker, R. H., & White, R. L. 2003, AJ, 126, 1217

Eisenstein, D. J., et al. 2001, AJ, 122, 2267

Elvis, M., et al. 1994, ApJS, 95, 1

Fan, X., et al. 2004, AJ, 128, 515

Francis, P. J., Nelson, B. O., & Cutri, R. M. 2004, AJ, 127, 646

Francis, P. J., Whiting, M. T., & Webster, R. L. 2000, Publications of the Astronomical Society of Australia, 17, 56

Fukugita, M., Ichikawa, T., Gunn, J. E., Doi, M., Shimasaku, K., & Schneider, D. P. 1996, AJ, 111, 1748

Glikman, E., Gregg, M. D., Lacy, M., Helfand, D. J., Becker, R. H., & White, R. L. 2004, ApJ, 607, 60

Goldschmidt, P., Kukula, M. J., Miller, L., & Dunlop, J. S. 1999, ApJ, 511, 612

Goldschmidt, P., & Miller, L. 1998, MNRAS, 293, 107

Goldschmidt, P., Miller, L., La Franca, F., & Cristiani, S. 1992, MNRAS, 256, 65P

Green, R. F., Schmidt, M., & Liebert, J. 1986, ApJS, 61, 305

Gunn, J. 2003, SDSS Photometric Equations, http://www.sdss.org/dr1/algorithms/jeg_photometric_eq_dr1

Gunn, J. E., et al. 1998, AJ, 116, 3040

Haas, M., et al. 2004a, A&A, 424, 531

Haas, M., et al. 2004b, A&A, 419, L49

Hall, P. B., et al. 2002, ApJS, 141, 267

Helfand, D. J., Stone, R. P. S., Willman, B., White, R. L., Becker, R. H., Price, T., Gregg, M. D., & McMahon, R. G. 2001, AJ, 121, 1872

Hewett, P. C., Foltz, C. B., & Chaffee, F. H. 1995, AJ, 109, 1498

Hogg, D. W., Finkbeiner, D. P., Schlegel, D. J., & Gunn, J. E. 2001, AJ, 122, 2129

Hopkins, P. F., et al. 2004, AJ, 128, 1112

Ivezić, Ž., et al. 2004, Astronomische Nachrichten, 325, 583

Ivezić, Ž., et al. 2002, AJ, 124, 2364

Kaspi, S., Smith, P. S., Netzer, H., Maoz, D., Jannuzi, B. T., & Giveon, U. 2000, ApJ, 533, 631

Kellermann, K. I., Sramek, R., Schmidt, M., Shaffer, D. B., & Green, R. 1989, AJ, 98, 1195

Kellermann, K. I., Sramek, R. A., Schmidt, M., Green, R. F., & Shaffer, D. B. 1994, AJ, 108, 1163

Kilkenny, D., O'Donoghue, D., Koen, C., Stobie, R. S., & Chen, A. 1997, MNRAS, 287, 867

Koratkar, A., & Blaes, O. 1999, PASP, 111, 1

Lacy, M., et al. 2004, ApJS, 154, 166

Landolt, A. U. 1973, AJ, 78, 959

—. 1983, AJ, 88, 439

—. 1992, AJ, 104, 372

Laor, A., Fiore, F., Elvis, M., Wilkes, B. J., & McDowell, J. C. 1997, ApJ, 477, 93

Liebert, J., Bergeron, P., & Holberg, J. B. 2004, ApJS, *in press* [astro-ph/0406657]

Lupton, R. H., Gunn, J. E., Ivezić, Z., Knapp, G. R., Kent, S., & Yasuda, N. 2001, in Astronomical Society of the Pacific Conference Series, 269–+

Lupton, R. H., Gunn, J. E., & Szalay, A. S. 1999, AJ, 118, 1406

Mickaelian, A. M., Gonçalves, A. C., Véron-Cetty, M. P., & Véron, P. 2001, Astrophysics, 44, 14

Miller, L., Peacock, J. A., & Mead, A. R. G. 1990, MNRAS, 244, 207

Miller, P., Rawlings, S., & Saunders, R. 1993, MNRAS, 263, 425

Oke, J. B., & Gunn, J. E. 1983, ApJ, 266, 713

Peacock, J. A., Miller, L., & Longair, M. S. 1986, MNRAS, 218, 265

Piconcelli, E., Jimenez-Bailon, E., Guainazzi, M., Schartel, N., Rodriguez-Pascual, P. M., & Santos-Lleo, M. 2005, å, in press [astro-ph/0411051]

Pier, J. R., Munn, J. A., Hindsley, R. B., Hennessy, G. S., Kent, S. M., Lupton, R. H., & Ivezić, Ž. 2003, AJ, 125, 1559

Porquet, D., Reeves, J. N., O'Brien, P., & Brinkmann, W. 2004, A&A, 422, 85

Richards, G. T., et al. 2001, AJ, 121, 2308

Richards, G. T., et al. 2003, AJ, 126, 1131

Richards, G. T., et al. 2002, AJ, 123, 2945

Sanders, D. B., Phinney, E. S., Neugebauer, G., Soifer, B. T., & Matthews, K. 1989, ApJ, 347, 29

Schmidt, M., & Green, R. F. 1983, ApJ, 269, 352

Schneider, D., et al. 2005, AJ, submitted

Schneider, D. P., Schmidt, M., & Gunn, J. E. 1994, AJ, 107, 1245

Schneider, D. P., et al. 2003, AJ, 126, 2579

Smith, J. A., et al. 2002, AJ, 123, 2121

Stoughton, C., et al. 2002, AJ, 123, 485

Strauss, M. A., et al. 2002, AJ, 124, 1810

Strittmatter, P. A., et al. 1980, A&A, 88, L12

Treister, E., et al. 2004, ApJ, in press [astro-ph/0408099]

Urry, C. M., & Padovani, P. 1995, PASP, 107, 803

Vanden Berk, D., et al. 2005, AJ, in press [astro-ph/0501113]

Vanden Berk, D. E., et al. 2001, AJ, 122, 549

Vanden Berk, D. E., et al. 2004, ApJ, 601, 692

Wampler, E. J., & Ponz, D. 1985, ApJ, 298, 448

Wandel, A., Peterson, B. M., & Malkan, M. A. 1999, ApJ, 526, 579

Warren, S. J., Hewett, P. C., & Foltz, C. B. 2000, MNRAS, 312, 827

White, R. L., Helfand, D. J., Becker, R. H., Gregg, M. D., Postman, M., Lauer, T. R., & Oegerle, W. 2003, AJ, 126, 706

Willott, C. J., Rawlings, S., Blundell, K. M., & Lacy, M. 1999, MNRAS, 309, 1017

Wisotzki, L., Christlieb, N., Bade, N., Beckmann, V., Köhler, T., Vanelle, C., & Reimers, D. 2000, A&A, 358, 77

Wolf, C., Wisotzki, L., Borch, A., Dye, S., Kleinheinrich, M., & Meisenheimer, K. 2003, A&A, 408, 499

York, D. G., et al. 2000, AJ, 120, 1579

Zakamska, N. L., et al. 2003, AJ, 126, 2125

This preprint was prepared with the AAS LaTeX macros v5.2.